

**ANTIVIRAL CHEMOTHERAPY FACILITATING CONTROL OF POXVIRUS INFECTIONS
THROUGH INHIBITION OF CELLULAR SIGNAL TRANSDUCTION**

Hailin Yang,^{1*} Sung-Kwon Kim,^{2*} Mikyung Kim,^{1*} Pedro A. Reche,^{1*} Tiara J. Morehead,³ Inger K. Damon,³ Raymond M. Welsh² and Ellis L. Reinherz¹

¹Laboratory of Immunobiology, Department of Medical Oncology, Dana-Farber Cancer Institute and Department of Medicine, Harvard Medical School, Boston, MA 02115

²Department of Pathology, University of Massachusetts Medical School, Worcester, MA 01655

³Poxvirus Section, Centers for Disease Control and Prevention, Atlanta, GA 30333

Address correspondence to Dr. Ellis L. Reinherz, Dana-Farber Cancer Institute, 44 Binney Street, Boston, MA 02115; phone 617-632-3412; fax 617-632-3351

email: ellis_reinherz@dfci.harvard.edu

*Equivalent contributors

Abbreviations: CAV, cell-associated virus; EEV, extracellular enveloped virus; EGF, epidermal growth factor; EGFR, epidermal growth factor receptor; IMV, intracellular mature virus; MGF, myxoma growth factor; SPGF, smallpox growth factor; TGF β , transforming growth factor β ; VGF, vaccinia growth factor; VV, vaccinia virus; WR, Western Reserve

ABSTRACT

The EGF-like domain of smallpox growth factor (SPGF) targets human erbB-1, inducing tyrosine phosphorylation of certain host cellular substrates via activation of the receptor's kinase domain and thereby facilitating viral replication. Given these findings, low molecular weight organic inhibitors of erbB-1 kinases might function as anti-viral agents against smallpox. Here we show that CI-1033 and related 4-anilinoquinazolines inhibit SPGF-induced human cellular DNA synthesis, protein tyrosine kinase activation and c-cbl association with erbB-1 and resultant internalization. Infection of monkey kidney BSC-40 and VERO-E6 cells in vitro by variola strain Solaimen is blocked by CI-1033 primarily at the level of secondary viral spreading. In an in vivo lethal vaccinia virus pneumonia model, CI-1033 alone promotes survival of animals, augments systemic T cell immunity and, in conjunction with a single dose of anti-L1R intracellular mature virus (IMV) particle-specific mAb, fosters virtually complete viral clearance from lungs of infected mice by day 8 post-infection. Collectively, these findings show that chemical inhibitors of host signaling pathways exploited by viral pathogens represent potent anti-viral therapeutics.

INTRODUCTION

Chemotherapeutic approaches to the control of viral infections have been less successful than those against bacterial infections because of the need of viruses to replicate in host cells and the attendant difficulty in selectively targeting the virus without damaging the host. To date, virtually all strategies for the development of antiviral drugs have focused on unique properties of the viral replicative cycle or of viral proteins that can be selectively targeted (1-3). These drugs include nucleoside analogues, and inhibitors of viral polymerase, protease, and fusion proteins. Most of the antiviral drugs currently in use are directed against persistently infecting viruses, such as HIV, where therapy is expected to continue for a long duration. Acute viral infections, however, may need only a short period of drug treatment to shift the balance between overwhelming and lethal virus load on the one hand and an effective and protective immune response on the other. Because viruses are dependent on host cell functions for their replication, we questioned whether a transient and well-tolerated interference of the normal functions of the cell types in which the virus replicates may retard viral replication and/or spread and spare the host from morbidity or mortality using poxviruses.

Smallpox was due to infection with variola major or variola minor of the orthopox genus, which belong to the poxvirus family of large double-stranded DNA viruses replicating in the cytoplasm of infected cells (4). Cessation of vaccination efforts more than two decades ago has resulted in susceptibility of a large segment of the population to this pathogen (5). This vulnerability requires additional methods to rapidly contain any future outbreak of infections with this group of viruses.

Epidermal growth factor (EGF)-like growth factors are carried by poxviruses to facilitate viral pathogenesis. Prominent skin manifestations elicited by a number of these viruses are probably linked to this gene product (4). Prior gene deletion studies showed that vaccinia growth factor (VGF) of the variola-related orthopox vaccinia virus (VV), contributes to virulence following intracranial inoculation of mice and intradermal inoculation of rabbits (6). Likewise, inactivation of myxoma growth factor (MGF) in the distantly-related leporipoxvirus diminishes viral-induced proliferation of epithelial cell layers in conjunctival and respiratory tracts (7). Since smallpox growth factor (SPGF) uses erbB-1 to

stimulate host cells (8), thereby aiding viral replication, we reasoned that if the viral factor's stimulatory activity was blocked, then viral growth might be curtailed.

The erbB 1-4 molecules are members of the receptor tyrosine kinase superfamily sharing common structural features including an extracellular ligand-binding domain, transmembrane segment and intracellular protein tyrosine kinase domain (9 and references therein). These receptors mediate physiologic growth factor signaling by EGF, transforming growth factor α (TGF α), epiregulin, amphiregulin and neuregulin among other growth factors. Although related, differences in their substrate specificity, signaling properties and physiology are evident. erbB-2 has no known extracellular ligand, and tyrosine kinase activity is absent in erbB-3. In addition, heterodimerization and homodimerization of erbB members contribute to signaling complexity, forming a multi-layered network of functional interaction in higher eukaryotes, unlike the single, primordial erbB homologue found in *C. elegans* and *Drosophila* (9). Since in excess of 60% of human tumors contain erbB abnormalities including receptor overexpression via gene amplification and/or rearrangements and erbB receptor-specific ligand aberrations which contribute to the malignant phenotype (9), approaches have been developed to block erbB signal transduction. In this regard, clinical inhibitors of erbB receptor tyrosine kinase pathways are being extensively investigated as anti-cancer agents in many human malignancies (10, 11).

The present study was conducted to determine whether such inhibitors might block orthopox infection and effects of the EGF-like pathogenic factors in vitro and in vivo. We show here that chemical interference with the signal transduction mediated by erbB-1 can lead to the control of variola virus in vitro and of vaccinia virus in vivo. Thus, targeting of a host cell signal transduction function needed for viral replication can be used as a new approach to antiviral chemotherapy.

RESULTS AND DISCUSSION

Identification of the 4-anilinoquinazoline CI-1033 as an inhibitor for SPGF action

Given the high affinity of SPGF for erbB-1 ($K_d = 0.14$ nM) (8), we evaluated several tyrosine kinase inhibitors belonging to the 4-anilinoquinazolines with strong selective specificity for erbB (Figure 1A). The structure of the erbB-1 receptor kinase domain alone and in complex with one such inhibitor indicates how these 4-anilinoquinazolines bind to the ATP-binding pocket of the kinase domain (12). Figure 1A shows that PD153035 and PD168393 have an identical 4-(3'-bromo-aniline) ring but differ in the R3 and R4 groups attached to the quinazoline ring. In particular, PD168393 has an acrylamide at position 6 which can alkylate erbB-1 Cys⁷⁷³ so that the inhibitor irreversibly binds to erbB-1 at a 1:1 molar ratio. The tyrosine kinase active erbB-2 and erbB-4 molecules have comparable cysteine residues at Cys⁷⁸⁴ and Cys⁷⁷⁸, respectively, which can be targeted for modification. In contrast, PD153035 binds in a reversible manner, primarily via hydrophobic forces. CI-1033, like PD168393, has the R3 acrylamide adduct at the 6 position as well as the solubilizing morpholine side chain at the 7 position (R4). CI-1033 demonstrates IC₅₀ values of 0.8, 19 and 7 nM for erbB-1, erbB-2 and erbB-4, respectively (13). Figure 1B represents our optimized molecular model for the binding of CI-1033 into the ATP pocket cleft found between the two major lobes of the erbB-1 kinase domain, prior to and after formation of the Cys⁷⁷³ adduct (14) and is based on the crystal structure of the complex between the erbB-1 kinase domain and OSI-774, a chemically related 4-anilinoquinazoline (12).

To examine the effect of the 4-anilinoquinazolines on SPGF-triggered activation of human epithelial cells, a series of in vitro experiments was performed. As shown in Figure 2A, after overnight stimulation of human fibroblasts with various concentrations of recombinant SPGF produced and purified as detailed elsewhere (8), the number of cells entering S phase approaches 8%. Pre-treatment of cells for 1 h at 37°C with 50 nM concentrations of the indicated inhibitors blocks this increase in DNA synthesis. Figure 2B shows that these same compounds inhibit tyrosine phosphorylation of erbB-1 (150kD band) as well as additional substrates (120kD, 80kD, 60kD and 55kD) triggered by SPGF in HeLa cells. The Src family protein tyrosine kinase (PTK)-specific inhibitor PP2 does not block the phosphorylation of these

erbB-1 substrates even when used at 10 μ M. In contrast, addition of PD168393 or CI-1033 at 50 nM largely prevents SPGF-triggered phosphorylation while the effect with PD153035 is only modest at best. These results suggest that reversible inhibitors of kinase activity may be less efficient at blocking substrate tyrosine phosphorylation compared to irreversible inhibitors at the 50 nM concentration tested. Similar inhibition of tyrosine kinase phosphorylation was observed with the vaccinia VGF orthologue (data not shown).

The Figure 2C inset shows the distribution of erbB-1 receptors in human HeLa epithelial cells prior to or 15 min after SPGF addition at 37°C as detected by immunofluorescence microscopy. In the absence of growth factor addition, the distribution of erbB-1 is primarily confined to the plasma membrane. In contrast, post-SPGF exposure, erbB-1 molecules are rapidly internalized, appearing as punctate intracellular fluorescent aggregates. To assess whether tyrosine kinase inhibitors influence the ability of SPGF to down-modulate erbB-1, A431 cells were pre-treated with inhibitors, incubated with biotinylated SPGF and shifted to 37°C for 5 min followed by fixation. Cell surface-bound erbB-1 ligand was then visualized with streptavidin-PE and quantitative fluorescence determined by FACS analysis. Without inhibitors, mean fluorescence intensity (MFI) was ~110 (Figure 2C). In contrast, the irreversible erbB inhibitors augment MFI ~3 fold (300-350) whereas the reversible erbB-1 inhibitor PD153035 increases MFI to 240. The src family kinase inhibitor PP2 only modestly affects erbB-1 surface copy number.

The erbB receptors are eliminated by two pathways: 1) ligand-dependent endocytosis and degradation involving a c-Cbl ubiquitin ligase mechanism (15) and 2) stress-induced shuffling of chaperones associated with these receptors and involving proteasomal proteinases (16). Recent studies show that erbB-2 kinase inhibition by CI-1033 promotes down-regulation of erbB-2 via the second process (17). However, given that CI-1033 enhances erbB-1 surface expression, the findings suggest that the effects of CI-1033 on ligand-specific down-regulation of erbB-1 expression are not analogous to those on constitutive erbB-2 expression. To examine if 4-anilinoquinazolines might influence c-Cbl interaction with erbB receptors, inhibitor pre-treated or untreated SPGF-stimulated HeLa cells were

immunoprecipitated with anti-erbB-1 antibodies. Subsequently, western blotting was performed with either anti-erbB-1 antiserum to quantitate expression of erbB molecules or with anti-c-Cbl to assess the effects of the compounds on erbB-1 association. As shown in Figure 2D, compared to unstimulated cells (-), the SPGF-triggered HeLa cells (+) have less total erbB-1 due to rapid intracellular degradation. Consistent with the FACS analysis (Figure 2C), PP2 has little influence on this process. On the other hand, PD153035, PD168393 or CI-1033 pre-treatment augments the total erbB-1 protein immunoprecipitated despite SPGF addition; note the several-fold increase in erbB-1 (i.e. EGFR) over the SPGF-unstimulated control cells. The latter result implies blockade of constitutive internalization/degradation of erbB-1 as well. More importantly, SPGF-inducible c-Cbl association with erbB is blocked by the 4-anilinoquinazolines but not by PP2. Loss of c-Cbl/erbB-1 complex formation is not secondary to reduction in total cellular c-Cbl levels as shown by parallel c-Cbl immunoprecipitation and western blotting. Instead, these erbB kinase inhibitors prevent the inducible association of c-Cbl with erbB-1 subsequent to SPGF binding.

Effect of CI-1033 on orthopox virus replication and spread

To examine the effect of CI-1033 on variola virus growth, a confluent monolayer of BSC-40 or VERO-E6 monkey kidney epithelial cells was infected with approximately 50 plaque-forming units of variola strain Solaimen in the presence or absence of various concentrations of the erbB inhibitor and cultured in vitro for 4 days. As shown in Figure 3A of the immunohistochemical-stained BSC-40 monolayer, increasing concentrations of CI-1033 dramatically reduce the size of the individual plaques and comet formation but with minimal effect on plaque number. This effect is titratable (Figure 3A, 3B, 3C), and at the highest concentration of 10 μ M, extremely small plaques are faintly visible. Although the total number of plaques at the highest concentrations of compound appears to decrease, the difference is not statistically significant ($p > 0.05$) when compared to seven randomly selected control wells (Figure 3A, 3B). Figure 3C illustrates a statistically significant decrease in the number of comets ($p < 0.05$) at CI-1033 concentrations of 500 nM or greater. Comets are representative of extracellular enveloped virus (EEV)

formation and dissemination (15). Similar qualitative observations are made when vaccinia strain IHDJ plaque morphology is observed (Figure S1). A role for VGF is implied by the somewhat smaller plaque size and markedly reduced comet formation observed with the vaccinia virus growth factor deletion mutant (vSC20, i.e. VGF⁻) relative to its WR parent as demonstrated on the BSC40 cells (Figure S1 inset) and VERO-E6 (data not shown). At concentrations up to 1 μ M CI-1033, no effect is observed on the minimal comets made by vSC20 but clear reduction in comet formation is evident for WR (Figure S1 inset).

Consistent with these findings, a single step growth curve of variola strain Solaimen in VERO-E6 cells demonstrates a delay in EEV formation (see Figure 3D, left panel), and a net reduction in EEV numbers by >2 logs at 10 μ M CI-1033. Less than one log decrease in the overall amount of cell-associated virus (CAV), comprising IMV and cell-associated enveloped viral particles, was observed (Figure 3D, right panel). Evaluating single step growth curve kinetics in BSC-40 cells demonstrates a less dramatic 1-2 log decrease in EEV with 10 μ M CI-1033 (data not shown). Kinetic evaluation of levels of viral DNA (Figure 3E) in VERO-E6 cells under conditions of high multiplicity infection shows no inhibition of viral DNA accumulation. No evidence of cytotoxicity due to 500 nM or 10 μ M CI-1033 was observed in uninfected BSC-40 cells or VERO-E6 cells by either a lactate dehydrogenase assay (Table 1, supplement) or trypan blue uptake (data not shown). These aggregate results suggest that CI-1033 does not block primary entry and initiation of viral replication but rather some specific step(s) in viral morphogenesis. Functionally, the release of EEV appears sensitive to inhibition. Orthopox viruses use both microtubule and actin filaments for egress (16, 17) with CEV inducing actin tails to eject themselves from the cell. As erbB-1 activation reorganizes the actin microfilament system (18), it appears likely that both cell-associated enveloped virus and extracellular enveloped virus release is blocked, retarding secondary virus cell-to-cell spread and hence limiting the size of individual plaques.

Note that the specificity of CI-1033 for erb family members is ~100,000 fold greater than for unrelated kinases such as PDGF receptor, FGF receptor, insulin receptor, cyclins D1, A and B (13, 14). This makes a "non-specific" effect extremely improbable for doses of CI-1033 \leq 1 μ M. On the other hand,

inhibition of the VGF- WR variant at the two highest drug concentrations (Figure S1 inset) implies either that additional endogenous growth factor signaling via EGFR is blocked or that inhibition of other viral-egress relevant tyrosine kinase activation cascades has occurred. By extension, this mechanism(s) applies to vaccinia IHDJ and WR and variola viruses. The more profound related effect on long range dissemination of virus via EEV potentially suggests additional mechanisms of interference. Because EGFR endocytosis is also linked to the actin cytoskeleton (18), erbB-1 kinase inhibition may serve to maintain surface EGFR expression via this mechanism as well (Figure 2C). More importantly, the ability of CI-1033 to block EGFR activation by cellular erbB ligands or trans-stimulation of erbB-1 via other receptors as well as its downstream effects on cytoskeletal elements used for poxviruses egress likely accounts for the profound effect on plaque morphogenesis not observed with anti-SPGF mAb (8).

Control of VV infection in vivo by CI-1033

Disruption of the VGF gene in vaccinia Western Reserve (WR) was shown to reduce pathogenicity of vaccinia virus in vivo by inhibiting viral growth and shifting the LD₅₀ 2,000 fold (6). Since CI-1033 blocks SPGF-stimulated erbB-1 driven cell growth, receptor-mediated tyrosine phosphorylation, internalization and degradation and in view of its anti-viral activity in vitro noted above, we reasoned that the erbB-1 kinase inhibitor may attenuate orthopox growth factor activity in vivo. To test this possibility, the effect of CI-1033 on the clinical course of B6 mice given an intranasal vaccinia WR challenge (19) was examined. This dose was close to the LD₅₀, so there was some variation in lethality between different experiments with mice of slightly different ages. Figure 4A shows an experiment with 7 week-old mice inoculated with 10⁴ PFU in which all (5/5) untreated mice died by day 7 post-infection from a fulminant acute pneumonia. In contrast, i.p. administration of CI-1033 at 50 mg/kg beginning 6 h prior to infection and continuing daily for 8 days completely prevented death. In a second experiment with 9 week-old mice inoculated with 10⁴ PFU in which drug treatment was stopped at day 5, 3/4 control mice were dead by day 9, but 5/5 drug-treatment mice remained alive at day 10

though eventually 3/5 had succumbed by day 14 (figure not shown). In a third experiment with 5 week old mice receiving 2×10^4 PFU, in which drug treatment stopped after 7 days, 4/4 untreated and 0/5 drug-treated mice died by day 9. 2/5 treated mice died at day 10, and 3/5 survived indefinitely (figure not shown). These experiments indicated that treatment with the drug alone could consistently either delay or inhibit death in response to this lethal dose of virus. Treatment with a single 200 μ g i.p. dose of anti-L1R vaccinia virus mAb (7D11) known to neutralize the IMV particles could also protect mice from the lethal effects of intranasal inoculation, as could combined anti-L1R and CI-1033 treatment (Figure 4A). Clinical monitoring of animals post-infection showed, however, that combined treatment with anti-L1R and CI-1033 reduced symptomatology significantly better than either treatment alone (Figure 4B). The efficacy of combined treatment was further illustrated in an experiment where 8 week old mice were given a higher dose of 5×10^4 PFU VV. Mice in all groups died except those with combined therapy, where 80% (4/5) survived.

A cohort of animals was sacrificed at 8 days post-infection and their lungs examined. Differences among gross lung weight in each treatment group are shown in Figure 4C. Untreated animals had edematous lungs with multiple hemorrhages weighing nearly two times that of normal, uninfected B6 lungs. This pathology is somewhat attenuated by anti-L1R or CI-1033 treatment alone but dramatically ameliorated by the combination of CI-1033 plus anti-L1R (see supplemental Figure S2). In five experiments, treatment with CI-1033 alone (1 mg/day) only modestly reduced viral lung titers compared to untreated infected controls [day 6a \square 0.42; day 6b \square 0.14; day 7 \square 0.20; day 8a \square 0.08; day 8b \square 0.50 \log_{10} PFU (where "a" and "b" refer to independent experiments)]. This contrasts with the more efficacious anti-L1R in the same experiments (day 6a \square 1.1; day 6b \square 0.54; day 7 \square 1.2; day 8a \square 2.2; day 8b \square 5.0 \log_{10} PFU). Combined treatment, however, tended to reduce viral titers by greater amounts as shown in these experiments (day 6a \square 1.4; day 6b \square 1.3; day 7 \square 2.9; day 8a \square 5.1; day 8b \square 5.4 \log_{10} PFU). In these experiments when control mice survived, and in another (Figure 4D) where control mice died, we noted that combined treatment was particularly effective at reducing viral titers by day 7-8 post-

infection. We have previously observed that mAb to SPGF, which cross-reacts with VGF, can also synergize with anti-L1R to reduce VV lung titers by day 8 (8). Figure 4D shows the enhancing effects of anti-SPGF and of CI-1033 in combination with anti-L1R at 8 days post-infection in an experiment where untreated control animals have died and cannot be titrated for infectivity (although 7-8 log₁₀ PFU are observed in other experiments). Thus, the CI-1033 drug can apparently replace anti-SPGF mAb in therapy against VV. The further two log viral titer reduction with anti-L1R plus CI-1033 compared with anti-L1R plus anti-SPGF therapy noted in Figure 4D may be a consequence of the irreversible binding of the drug (14) compared with reversible mAb binding, affording a more complete blockade of the erbB-1 pathway along with inhibition of endogenous host erb-B ligands. Another explanation may be that CI-1033 blocks dissemination of EEV. In vivo pharmacokinetic studies in mice at the dose range employed herein show peak plasma levels of CI-1033 of 2.2 μ M, a concentration inhibiting comet formation in vitro (Figure 3 and data not shown).

We consistently noted that mice treated with CI-1033 alone or in combination with anti-IMV mAb had less morbidity and looked much healthier than non-drug-treated controls, even under conditions when there were only minor differences in lung viral titers. This may have been due in part to the more effective control of the progression of infection in other organs. In the liver, for example, there were nearly 100-fold lower titers of virus in drug-treated groups by day 5 post-infection (D5 control = 4.6 vs. drug-treated = 2.8 log₁₀ PFU, p = .02; D7 control = 4.7 vs. drug-treated = 3.0 log₁₀ PFU, p = .003). Correspondingly, the number and size of inflammatory foci in the livers were much reduced in the drug-treated mice.

Augmentation of anti-viral host response

In the combination anti-L1R plus anti-SPGF immunotherapy model (8), augmented T cell responses to VV were detected by day 6 post-infection. To determine whether CI-1033 alone or in combination with anti-L1R may augment T cell responses, we examined T cell-regulated cytokine production in lungs by RNase protection analysis at days 4, 6 and 8 post-infection. As shown in Figure

S3A (supplemental data), compared to untreated mice, CI-1033 alone augments IL-1 β , IL-1 receptor antagonist (IL-1Ra) and IFN- γ peaking at day 6, without influencing IL-6, IL-10, IL-12 or MIF. For example, the IFN- γ signal is 4.1 fold greater on day 6 with CI-1033-treated mice relative to the control-infected animals. Consistent with the lung cytokine level, systemic antigen-specific T cell responses to VV-infected MC57G fibroblasts (H-2^b) are augmented substantially by CI-1033 relative to control untreated mice as judged by splenic CD8⁺CD44⁺ intracellular IFN- γ production (Figure S3B). The percentage of VV-MC57G activated IFN- γ -producing CD8 T cells is 10-fold higher than untreated VV-infected mice on day 8 post-infection and this corresponds to a 21-fold increase in absolute number (1.85×10^5 vs. 8.5×10^3 cells). In the same experiment, 23- and 48-fold increases were observed for anti-L1R and anti-L1R + CI-1033 treated mice, respectively. That anti-L1R treatment leads to more IFN- γ cytokine RNA in the lung than the anti-L1R + CI-1033 dual therapy (Figure S3) may be indicative of persistent viral load, particularly at day 8 post-infection, with the former treatment (Figure 4D). In sum, chemotherapy alone and combination immunoprophylaxis/chemotherapy are efficient at reducing viral titer and stimulating T cell immunity. The latter may be a consequence of preventing the elaboration of anti-inflammatory viral products as well as later rounds of DNA virus replication in epithelial cells dependent on the viral growth factor (20, 21). As such, we perceive a linkage between viral growth, viral spreading and host immunity as modulated through SPGF/VGF and erbB-1 interaction.

Post-exposure therapy

Current interest in orthopox virus therapeutics stems from concerns that variola virus may be used as a bioterrorism agent. Hence, post-exposure therapy protocols may be needed as an alternative to post-exposure vaccination. We therefore tested the efficacy of CI-1033 as a post-exposure therapeutic agent, with and without mAb-dependent immunotherapy. The intranasal VV infection of mice rapidly progresses, unlike the slow incubation time for development of symptoms in humans after exposure to variola (4, 5). Successful therapy in this rapidly progressing VV murine model would thus provide promise for possible drug intervention of human infections. Mice (7-10 weeks of age) were therefore

inoculated i.n. with 2×10^4 PFU VV for two days to allow for substantial replication of VV, prior to subsequent therapeutic intervention. An initial survival experiment showed that drug treatment alone did not prevent lethality, which was prevented by mAb L1R, with or without CI-1033 (data not shown). Figure 5 summarizes results in three other experiments after 4 (day 6), 5 (day 7), and 6 (day 8) days of therapy. Drug alone provided no protection by itself by day 6, though it appeared to augment the protective effect of anti-L1R, in regards to reduced lung weight and lower lung titers. Those parameters did not reach statistical significance, but by this early time point a statistically significant increase in anti-CD3-induced IFN γ -producing CD8 T cells per spleen was seen with combined therapy. By day 7 the same trends were observed, with combined therapy resulting in lower lung weights and viral titers and now dramatically (6-fold) increased T cell responses. Clinical scores (scoring system as described in Methods and ref. 8) were substantially improved in the combined therapy group at day 7 (untreated = 4.0 +/- 0; L1R = 3.4 +/- 0.6; L1R + CI-1033 = 2.4 +/- 0.5). By day 8, 4/5 of the untreated controls had died, as expected. In comparison to L1R-treated mice, there were statistically significant reductions in lung viral titers ($p=.02$) in the combined therapy group, which also had reduced lung size, substantial splenomegaly, and more than three times the number of VV-specific T cells in the spleen. The heightened T cell response at day 8 allowed for the examination of VV-specific CD8 T cells, as determined by their production of IFN γ after incubation with VV-infected DC2.4 dendritic cells. VV-specific T cell responses were greater than 3-fold higher in mice receiving combined therapy ($11.4 \pm 3.3 \times 10^5$) than in those receiving only mAb L1R therapy ($3.2 \pm 4.2 \times 10^5$), $p = .002$. These experiments demonstrate the post-exposure efficacy of CI-1033 when used in combination with immunotherapy.

Implications

The use of host cellular signaling pathway blockade as a target for anti-viral chemotherapy is distinct from other approaches typically directed against pathogens themselves. One advantage of the host-targeted strategy is that drug resistance cannot develop. Furthermore, unlike with anti-SPGF mAbs (8) where cross-reactivity with other closely-related pathogenic factors (i.e. VGF vs. SPGF) are not

guaranteed, the erbB inhibitors are potentially able to block immunologically distinct ligands to various erbB PTK family members. This broader target activity is relevant since, for example, VGF and MGF bind distinct erbB receptors (22). Whether CI-1033 by itself would be a sufficient therapy against variola virus infection remains to be determined, but appears possible given that the dose of orthopox particle inhalation from natural or bioterrorist spread is likely to be less than that employed in the current study, and the time course for the progression of smallpox is much longer than in the VV-infected mouse model. In addition, the drug dosing/scheduling has yet to be optimized. How efficiently post-exposure therapy might thwart clinical infection now requires careful scrutiny. That CI-1033 augments T cell responses while reducing infectious symptomatology also suggests its consideration as an immune stimulant post-vaccinia vaccination with possible utility in treatment of complications of immunization. Other erbB inhibitors (23, 24) may also be useful in this regard.

Aside from poxviruses and their erbB-directed growth factors, hepatitis B virus and Epstein-Barr virus make products that dysregulate erbB-1 transcription (25, 26). RNA tumor viruses also exploit erbB-1 signaling (27). In addition, functional EGF receptors have been reported to be necessary for efficient reovirus (28) and human cytomegalovirus infection of host cells (29). These findings collectively suggest that multiple viral infections may be coupled to the erbB-mediated signaling network. Epithelial cells which constitutively or inducibly express erbB receptors are common sites of viral replication (30). Perhaps erbB inhibitors will have wider application in infectious diseases beyond those involving orthopoxviruses. Development of chemical inhibitors of cellular signaling pathways exploited by viral pathogenic factors may offer a new approach toward infectious disease control in general.

METHODS

Chemical inhibitors. CI-1033 was provided by Pfizer, Inc. PP2, PD153035 and PD168393 were purchased from Calbiochem.

Human fibroblast proliferation assay. Human foreskin fibroblasts (SC-J) were plated in 6 well plates and starved overnight in 2% FCS-DMEM medium, and then pretreated with inhibitors for 1 hour at 37°C followed by stimulation with different amounts of SPGF. 18 hours later, the cells were harvested and fixed in 80% ice-cold ethanol at 4°C for 1 h. After a single wash with PBS, cells were stained with 2.5 µg/ml propidium iodide and 50 µg/ml RNase A at 37°C for 30 min. Cell cycle data were collected by FACS analysis using Cellquest (Becton Dickinson) and analyzed by Modfit.

ErbB1 (EGFR) internalization. HeLa cells were cultured on chamber slides and stimulated with ligands (50 ng/ml) at 37°C for 10 min. Cells were then fixed using 3.7% formaldehyde for 10 min and permeabilized with 0.1% Triton X-100 for 5 min at room temp. Cells were stained with 1µg of anti-EGFR mAb (Santa Cruz Biotechnology Inc.) in 1%BSA/PBS at room temp for 30 min, followed by staining with anti-mouse Ig-FITC conjugates.

A431 epidermal carcinoma cells were pretreated with 50 nM inhibitors at 4°C for 30 min. 100 ng of biotinylated SPGF was incubated with the cells for a further 30 min at 4°C. After washing, cells were incubated at 37°C for 5 min and fixed in formaldehyde for 5 min at room temperature. Subsequent to streptavidin-PE staining, mean fluorescence intensity was obtained by FACS.

Cell lysate preparation, immunoprecipitation and western blotting. HeLa cells were treated with 50 nM inhibitors at 37°C for 30 min, followed by 50 ng/ml SPGF stimulation. Cell lysates were prepared and subjected to immunoprecipitation with anti-EGFR (goat polyclonal, Santa Cruz Biotechnology Inc.) and gamma-bind plus beads (Amersham Biosciences Corp.) or anti-c-Cbl beads (Santa Cruz Biotechnology Inc.) at 4°C overnight using previously described methods (8). Beads were washed and eluted in 2 X SDS-PAGE loading buffer and analyzed by western blotting with either anti-EGFR or anti-c-Cbl.

Vaccinia virus infection of mice. 4-10 week male C57BL/6 were injected intraperitoneally with

200 µg anti-L1R (7D11) mAb in PBS and/or 50 mg/kg/day CI-1033 in 0.05 N sodium lactate buffer, pH 4. Infected control mice were either treated with a control mAb in PBS or sodium lactate buffer without drug. Six hours later, mice were infected intranasally with 4×10^4 PFU vaccinia virus, WR strain. Each day the mice were weighed and observed for symptoms of infection (0 = normal, 1 = ruffled fur; 2 = 1 plus hunched position; 3 = 2 plus little locomotion; 4 = 3 plus lethargic and minimally responsive). Virus titer was determined by plaque assay on VERO cells as previously described (31). CI-1033 treatment was of 6-10 days duration. Intracellular cytokine staining of CD8 T cells was done as previously described, using either anti-CD3, VV-infected MC57G cells, or VV-infected DC2.4 dendritic cells (obtained from Dr. Ken Rock, UMass Medical School) to stimulate splenic lymphocytes (8). In some experiments mice were infected with VV two days prior to treatment with mAb and/or CI-1033. All animal experimentation was performed according to AAALAC approved protocols for ethical treatment.

Titration effect of CI-1033 on variola plaque and comet formation. Confluent BSC-40 monolayers were pre-treated or mock-treated in the presence or absence of CI-1033 in RPMI + 2% FBS (RPMI-2%) at varying concentrations in triplicate for 30 min at room temp. Seven concentrations of CI-1033 were evaluated, three mock-treated controls per each concentration of CI-1033 were performed on 7 individual 6-well plates. Monolayers were infected with a suspension of variola strain Solaimen in the presence or absence of CI-1033, such that ~50 pfu per well of virus were observed. Plates were incubated at 35°C, 6% CO₂ for 1 hr and rocked at 15 min intervals to insure an even infection of the monolayer. The inoculum was removed and the monolayer was rinsed 1x with RPMI-2%. The monolayers were over-laid with medium +/- CI-1033 at the appropriate concentrations and incubated at 35°C, 6% CO₂ for 4 days. **The plates were then gamma-irradiated at the kill dose (4.4×10^6 rads) and removed from the BSL-4 laboratory for immunohistochemical staining.** Plaques were immunohistochemically stained for analysis. Comets were defined as greater than two or more successively smaller plaques in comet-shaped association with a large plaque. The number of plaques and comets in the presence of different

concentrations of CI-1033 were compared to control plates by using a Wilcoxon rank-sum test. Seven randomly selected mock-treated wells, one selected from each of seven plates, were used for comparison.

Molecular modeling. CI-1033 was docked into the ATP binding site of the kinase crystal structure (12) manually using the information that the compound bound irreversibly to Cys773 (14). The modeling was performed with the Sybyl molecular modeling package using the standard minimizer (Maximin) with the Tripos force field, hydrogen atoms were included, and minimizations were done without charges on any atoms (Tripos Associates, Inc. <http://www.tripos.com/>). The quinazoline ring of CI-1033 was placed in the same orientation and docking mode as observed for Tarceva, another erbB inhibitor (12). Distance constraints from the quinazoline N1 to the Met769 backbone NH kept these atoms within hydrogen bonding distance. Also distance constraints kept the C2 hydrogen of the quinazoline ring and the carbonyl oxygen of Gln760 to the distance observed in the crystal structure. Torsional constraints were employed to keep the core ring fully planar. CI-1033 was manually placed in the ATP binding site, and the complex minimized, first with the protein aggregated to allow the ligand to fit the pocket after manual docking, then with the constraints removed and minimized for 400 iterations.

For the covalently bound variant, the initial modeling of the non-covalently bound variant was the starting point. The sidechain of the CI-1033 molecule was oriented close to the Cys773 sulfur and the appropriate bond formed. All atoms but the ligand and the Cys773 were formed into an aggregate and the system was minimized. This allowed only the ligand and Cys773 atoms to move. After minimization with the aggregate, the aggregate was removed and the full system was allowed to minimize for 400 iterations, still maintaining the distance and torsional constraints.

RNase protection assay. One lobe of lung from each treated mouse at various days post-infection was disrupted in RLT buffer (Qiagen Inc.) through an 18 gauge needle. Lysates were further homogenized by QIAshredder modules and purified using an RNeasy Mini kit according to the manufacturer's protocol (Qiagen Inc.). Equal amounts of total RNA (2 μ g/mouse) were pooled from three mice at each time point (days 4, 6 and 8). Six μ g were hybridized and processed with probes made from the mCK-2b template set according to the manufacture's protocol (BD Pharmingen).

Variola single-step growth curve in BSC-40 and VERO-E6 Cells. Confluent BSC-40 and VERO-E6 monolayers were pre-treated or mock-treated in the presence or absence of CI-1033 in RPMI + 2% FBS at 500 nM and 10 μ M concentrations for 30 min at room temp. Monolayers were infected at a MOI of 10 with a suspension of variola strain Solaimen in the presence or absence of CI-1033 at the appropriate concentrations. Plates were incubated at 35°C, 6% CO₂ for 1 h and rocked at 15 min intervals to insure even infection of the monolayer. The inoculum was removed and the monolayer was rinsed 2x with RPMI-2%. The monolayers were over-laid with media +/- CI-1033 at the appropriate concentrations and incubated at 35°C, 6% CO₂. Extracellular enveloped virus (EEV) and CAV were harvested from independent wells in triplicate at various timepoints post infection.

Titration harvested samples. EEV was harvested by removing a 100 μ l aliquot of the infection supernatant and serially diluting in 900 μ l RPMI-2% + IMV-neutralizing J2D5 mAb (1:1000). This concentration of mAb was demonstrated to neutralize 99% of IMV. Dilutions were then plated onto confluent VERO-E6 cell monolayers and incubated at 35°C, 6% CO₂ for 1 h and rocked at 15 min intervals to insure even infections of the monolayer. The inoculum was removed and the monolayers were overlaid with 2 ml RPMI-2% + J2D5 mAb. Plates were incubated at 35°C, 6% CO₂ for 4 days and stained with an equal volume of 2x Crystal Violet. Viral titer was determined by counting plaques. CAV was harvested by removing the remaining infection supernatant after EEV harvest and adding 1 ml fresh RPMI-2% to each well. The CAV samples were then titrated using a standard method for orthopox plaque assay (32). A 1ml aliquot was placed into a labeled tube and stored at -80°C until titered.

Viral DNA load. Viral DNA was isolated from CAV timepoint samples using a slight variation of the BIORAD Genomic DNA Isolation Protocol (Biorad Laboratories). Viral DNA load was determined using a Real-Time PCR method that targets the orthopoxvirus DNA polymerase. Details are available upon request.

Cytotoxicity assay. A confluent BSC40 or VERO-E6 cell monolayer was grown in a six-well plate and treated with various concentrations of CI-1033 in 2ml RPMI-2%. The plate was incubated at

37°C, 6% CO₂ for 48 hours. Media was removed from the cell monolayers and placed into corresponding labeled tubes, and an additional 2ml RPMI-2% was added to each well. Using a 1cc syringe barrel, cell monolayers were scraped into suspension and the removed to labeled tubes. The cell resuspension samples were lysed using the freeze/thaw method, followed by centrifugation of all samples collected at 250 x g for 5 minutes. Cytotoxicity was measured using the CytoTox 96 Non-Radioactive Cytotoxicity Assay Kit and protocol (Promega Corp.). Absorbance was read at 490 nm and percent cytotoxicity was determined and expressed as the amount of experimental LDH released into the medium +/- CI-1033 divided by the maximum possible amount of LDH released by lysing of the cells (experimental LDH release / maximum LDH release). Alternatively, after 48 h, an equal volume of Trypan Blue stain was added to each well. Cells were stained for 10 minutes at room temperature. Stain was removed from the cell monolayer and cells were observed under a microscope for any evidence of stain absorption, indicating cellular membrane permeability and death.

Online supplemental material: Figure S1 shows vaccinia virus IHDJ comet formation and inhibition by CI-1033 in BSC40 and VERO-E6 cells. Figure S1 inset shows vaccinia virus WR and VGF deletion mutant (vSC20) comet formation and inhibition by CI-1033 in BSC40 cells. Figure S2 provides hematoxylin and eosin staining of lungs from VV-infected mice in untreated and experimental groups. Figure S3 examines whole lung cytokine expression profiles and IFN- γ production in CD8⁺ T cells in these groups. Table S1 shows minimal to no cytotoxicity of CI-1033 in experiments performed in parallel with the plaque morphology experiments in Figure S1. Methods of preparation of rabbit anti-variola hyperimmune sera and immunohistochemical staining of variola plaques are given.

Acknowledgements

This work was supported by NIH grants AI50900, AI19807 and a grant from the Dana Foundation to ELR and NIH grant AR-35506 to RMW. The authors state no conflict of interest exists. We thank Drs. David Fry, Huifen Chen and James B. Dunbar for molecular modeling efforts and helpful discussions. We acknowledge scientific input from Drs. Miles Brown, Ray Dolin, Wayne Klohs and Barrett Rollins. We also acknowledge Dr. Aaron Curns for statistical support. **We thank Dr. Bernard Moss for providing WR and vSC20 vaccinia virus strains.**

REFERENCES

1. Balfour, H.H. 1999. Antiviral drugs. *N Engl J Med* **340**:1255-1268.
2. Dolin, R. 2001. Antiviral chemotherapy, excluding antiretroviral drugs. In *Principles of Internal Medicine*. E. Braunwald, A.S. Fauci, D. Kasper, S.L. Hauser, D.L. Longo, and J.L. Jameson, editors: McGraw-Hill. 1092-1100.
3. Fauci, A.S., and Lane, H.C. 2001. Human immunodeficiency virus (HIV) disease: AIDS and related disorders. In *Principles of Internal Medicine*. E. Braunwald, A.S. Fauci, D. Kasper, S.L. Hauser, D.L. Longo, and J.L. Jameson, editors: McGraw-Hill. 1852-1913.
4. Fenner, F., Wittek, R., and Dumbell, K.R. 1988. *The orthopoxviruses*. San Diego: Academic Press.
5. Henderson, D.A., Inglesby, T.V., Bartlett, J.G., Ascher, M.S., Eitzen, E., Jahrling, P.B., Hauer, J., Layton, M., McDade, J., Osterholm, M.T., et al. 1999. Smallpox as a biological weapon: Medical and public health management. *JAMA* **281**:2127-2137.
6. Buller, R.M., Chakrabarti, S., Cooper, J.A., Twardzik, D.R., and Moss, B. 1988. Deletion of the vaccinia virus growth factor gene reduces virus virulence. *J Virol* **62**:866-874.
7. Opgenorth, A., Nation, N., Graham, K., and McFadden, G. 1993. Transforming growth factor alpha, Shope fibroma growth factor, and vaccinia growth factor can replace myxoma growth factor in the induction of myxomatosis in rabbits. *Virol* **192**:701-709.
8. Kim, M., Yang, H., Kim, S.-K., Reche, P.A., Tirabassi, R.S., Hussey, R.E., Chishti, Y., Rheinwald, J.G., Morehead, T.J., Damon, I., et al. 2004. Biochemical and functional analysis of smallpox growth factor (SPGF) and anti-SPGF monoclonal antibodies. *J Biol Chem* **279**:25838-25848.
9. Yarden, Y., and Sliwkowski, M.X. 2001. Untangling the erbB signalling network. *Nat Rev Mol Cell Biol* **2**:127-137.
10. Cockerill, G.S., and Lackey, K.E. 2002. Small molecule inhibitors of the class I receptor tyrosine kinase family. *Curr Top Med Chem* **2**:1001-1010.

11. Wakeling, A.E. 2002. Epidermal growth factor receptor tyrosine kinase inhibitors. *Curr Opin Pharmacol* **2**:382-387.
12. Stamos, J., Sliwkowski, M.X., and Eigenbrot, C. 2002. Structure of the epidermal growth factor receptor kinase domain alone and in complex with a 4-anilinoquinazoline inhibitor. *J Biol Chem* **277**:46265-26272.
13. Allen, L.F., Lenehan, P.F., Eiseman, I.A., Elliott, W.L., and Fry, D.W. 2002. Potential benefits of the irreversible pan-erbB inhibitor, CI-1033, in the treatment of breast cancer. *Sem Oncol* **29**:11-21.
14. Fry, D.W., Bridges, A.J., Denny, W.A., Doherty, A., Greis, K.D., Hicks, J.L., Hook, K.E., Keller, P.R., Leopold, W.R., Loo, J.A., et al. 1998. Specific, irreversible inactivation of the epidermal growth factor receptor and erbB2, by a new class of tyrosine kinase inhibitor. *Proc Natl Acad Sci USA* **95**:12022-12027.
15. Soubeyran, P., Kowanetz, K., Symkiewicz, I., Langdon, W.Y., and Dikic, I. 2002. Cb1-CIN85-endophilin complex mediates ligand-induced downregulation of EGF receptors. *Nature* **416**:183-187.
16. Xu, W., Mimnaugh, E., Rosser, M.F., Nicchitta, C., Marcu, M., Yarden, Y., and Neckers, L. 2001. Sensitivity of mature ErbB2 to geldanamycin is conferred by its kinase domain and is mediated by the chaperone protein Hsp90. *J Biol Chem* **276**:3702-3708.
17. Citri, A., Alroy, I., Lavi, S., Rubin, C., Xu, W., Grammatikakis, N., Patterson, C., Neckers, L., Fry, D.W., and Yarden, Y. 2002. Drug-induced ubiquitylation and degradation of ErbB receptor tyrosine kinases: implications for cancer therapy. *EMBO J* **21**:2407-2417.
18. Lynch, D.K., Winata, S.C., Lyons, R.J., Hughes, W.E., Lehrbach, G.M., Wasinger, V., Cordwell, S., and Daly, R.J. 2003. A Cortactin-CD2-associated protein (CD2AP) complex provides a novel link between epidermal growth factor receptor endocytosis and the actin cytoskeleton. *J Biol Chem* **278**:21805-21813.

19. Chen, H.D., Fraire, A.E., Joris, I., Brehm, M.A., Welsh, R.M., and Selin, L.K. 2001. Memory CD8+ T cells in heterologous antiviral immunity and immunopathology in the lung. *Nat Immunol* **2**:1067-1076.
20. Alcami, A. 2003. Viral mimicry of cytokines, chemokines and their receptors. *Nat Rev Immunol* **3**:36-50.
21. Seet, B.T., Johnston, J.B., Brunette, C.R., Barrett, J.W., Everett, H., Cameron, C., Spypula, J., Nazarian, S.H., Lucas, A., and McFadden, G. 2003. Poxviruses and immune evasion. *Ann Rev Immunol* **21**:377-423.
22. Tzahar, E., Moyer, J.D., Waterman, H., Barbacci, E.G., Bao, J., Levkowitz, G., Shelly, M., Strano, S., Pinkas-Kramarski, R., Pierce, J.H., et al. 1998. Pathogenic poxviruses reveal viral strategies to exploit the ErbB signaling network. *EMBO J* **17**:5948-5963.
23. Fry, D.W., Kraker, A.J., McMichael, A., Ambroso, L.A., Nelson, J.M., Leopold, W.R., Connors, R.W., and Bridges, A.J. 1994. Specific inhibitor of the epidermal growth factor receptor tyrosine kinase. *Science* **265**:1093-1095.
24. Levitzki, A., and Gazit, A. 1995. Tyrosine kinase inhibition: an approach to drug development. *Science* **267**:1782-1788.
25. Menzo, S., Clementi, M., Alfani, E., Bagnarelli, P., Iacovacci, S., Manzin, A., Dandri, M., Natoli, G., Levrero, M., and Carloni, G. 1993. Transactivation of epidermal growth factor receptor gene by the hepatitis B virus X-gene product. *Virology* **196**:878-882.
26. Miller, W.E., Earp, H.S., and Raab-Traub, N. 1995. The Epstein-Barr virus latent membrane protein 1 induces expression of the epidermal growth factor receptor. *J Virol* **69**:4390-4398.
27. Adelsman, M.A., Huntley, B.K., and Maihle, N.J. 1996. Ligand-independent dimerization of oncogenic v-erbB products involves covalent interactions. *J Virol* **70**:2533-2544.
28. Strong, J.E., Tang, D., and Lee, P.W.K. 1993. Evidence that the epidermal growth factor receptor on host cells confers reovirus infection efficiency. *Virology* **197**:405-411.

29. Wang, X., Huong, S.-M., Chiu, M.L., Raab-Traub, N., and Huang, E.-S. 2003. Epidermal growth factor receptor is a cellular receptor for human cytomegalovirus. *Nature* **424**:456-461.
30. Yoo, J.-Y., and Desiderio, S. 2003. Innate and acquired immunity intersect in a global view of the acute-phase response. *Proc Natl Acad Sci USA* **100**:1157-1162.
31. Selin, L.K., Varga, S.M., Wong, I.C., and Welsh, R.M. 1998. Protective heterologous antiviral immunity and enhanced immunopathogenesis mediated by memory T cell populations. *J Exp Med* **188**:1705-1715.
32. Earl, P.L., Cooper, N., and Moss, B. 1993. Titering a vaccinia virus stock using a plaque assay. *Curr Prot Mol Biol Section IV*:16.16.15.

FIGURE LEGENDS

FIGURE 1 Structure of erbB tyrosine kinase inhibitors. A) Chemical structures of erbB tyrosine kinase inhibitors. B) Molecular model of CI-1033 interaction with the erbB-1 kinase domain. The upper panel shows the model of the non-covalently bound CI-1033 in the ATP binding site of the tyrosine kinase erbB-1 (PDB: 1M17) crystal structure. The Tarceva compound was removed and CI-1033 was manually modeled into the site. The backbone of the kinase is shown as a ribbon diagram along with the atoms of Cys773. The atoms are shown as stick models with carbon atoms colored white, oxygen atoms red, nitrogen atoms dark blue, sulfur atoms yellow, and hydrogen atoms colored light blue. The lower panel shows the model of the covalently bound CI-1033 in the ATP binding site.

FIGURE 2 erbB inhibitors block the function of SPGF. A) Inhibition of human foreskin fibroblast proliferation by erbB inhibitors. Human fibroblasts were starved in low serum-containing medium, then pretreated with 50 nM inhibitors at 37°C for 1 h followed by SPGF triggering overnight. Cells were analyzed by staining with propidium iodide and flow cytometry. Percentage of cells entering S phase is plotted. Grey area represents the baseline S phase after serum starvation. B) Inhibitors block cellular protein tyrosine phosphorylation triggered by SPGF. HeLa cells were pretreated with 50 nM inhibitors (PP2, 10 μ M) at 37°C for 30 min and then stimulated with 50 ng/ml SPGF at 37°C for 15 min. Minus (-) indicates no inhibitors or SPGF and plus (+) indicates SPGF addition only. Total cell lysates were analyzed by western blotting with 4G10 anti-phosphotyrosine mAb. Arrows indicate positions of phosphorylated substrates affected by erbB-1 inhibition. Numbers on left side of the panel indicate the molecular marker in KDa. C) erbB-1 internalization prevented by inhibitors. A431 cells were pretreated with inhibitors as above at 4°C for 30 min. Then 100 ng of biotinylated SPGF was incubated with cells for a further 30 min at 4°C. Cells were then washed, incubated at 37°C for 5 min to induce receptor internalization, then fixed and visualized with streptavidin-PE. Mean fluorescence intensity (MFI) is recorded. Results are representative of three independent

experiments. The inset shows the erbB-1 cellular distribution pattern in HeLa cells in the absence (-) or presence of SPGF. D) Inhibitors block association of erbB-1 and c-Cbl and subsequent erbB-1 degradation. HeLa cells were pretreated with inhibitors and stimulated (37°C, 5 min) with SPGF as above. Total cell lysates were immunoprecipitated (IP) with anti-EGFR or anti-c-Cbl and subjected to western blot (WB) with either antibody.

FIGURE. 3 Prevention of secondary variola virus spreading in vitro by erbB kinase inhibition. A) Immunohistochemical staining of variola strain Solaimen plaques on monolayers of BSC-40 cells after 4 days in the presence (+) or absence (-) of indicated molar concentrations of CI-1033. B) Titration effect of CI-1033 on variola plaque formation. C) Titration effect of CI-1033 on variola comet formation. Asterisks indicate statistically significant differences ($p < 0.05$) from seven randomly selected control wells. D) Time course of variola virus production (single step growth curve) on VERO-E6 cells in the absence (untreated) or presence of indicated concentration of CI-1033 with left and right panels showing EEV and CAV titers, respectively. E) Viral DNA genome copies from variola single step growth curve in VERO-E6 cell in the absence (untreated) or presence of 500 nM or 10 μ M CI-1033.

FIGURE 4 Rescue of mice from lethal vaccinia pneumonia by an erbB inhibitor. A) Mouse survival curves after intranasal vaccinia inoculation following pretreatment with CI-1033 (1 mg/mouse/day) and/or anti-L1R (200 μ g i.p. 6 h pre-inoculation). Note that all control mice died by day 7. Each treatment group includes a cohort of five animals. B) Clinical score of mice during treatment. The score (0-4) is explained in the Methods and is the mean value of the five mice per group. C) Average weight of the entire lung 6 days after lethal vaccinia infection with or without indicated treatment ($n = 3$ per group) vs. normal, uninfected lung. D) Virus titers in lungs at day 8 post-infection. Results are representative of five experiments.

FIGURE 5 Post-exposure therapy of VV-infection in the C57BL/6 pneumonia model. Mice were inoculated i.n. with 2×10^4 PFU of VV, and two days later treated with a single dose of mAb L1R or control mAb and/or with CI-1033, the latter given daily until termination of the

experiment. Mice were harvested on different days post-infection and examined for lung weight (A), VV PFU/lung (B), and the number of anti-CD3-induced IFN γ -producing CD8 T cells per spleen (C). For days 6, 7 and 8, group sizes of 3-4, 5 or 6 animals, respectively, were employed. At day 8, 2 of 6 anti-L1R-treated mice had undetectable virus, whereas 5/6 anti-L1R+CI-1033-treated mice had undetectable virus. For calculation of mean titers, the lowest possibly detectable titer (1 log) was used for mice without detectable virus, such that the means are actually lower values. * $p < .05$.

SUPPLEMENTAL MATERIAL

Preparation of rabbit anti-variola hyperimmune sera. Within BSL-4 containment, four rabbits were immunized with purified variola, strain Bangladesh. Immunizations, intradermal (ID) and subcutaneous (SC) were made over 4 axillary and inguinal regions with Freund's adjuvant, at day 0, and 29. Equal volumes of Freund's and a final volume of 1×10^9 pfu variola were used as the immunogen. Animals were euthanized and terminally bled 50 days post the second immunization; the terminal bleed was pooled with bleeds from 10 days, 20 days and 40 days post the second immunization to make the standard lot of pooled rabbit anti-variola hyperimmune sera. The sera was demonstrated to efficiently recognize variola, the 50% PRNT neutralization titer is extrapolated to be 1:1819 by the Kaber-Kogan method.

Immunohistochemical staining of variola and vaccinia plaques. Viral infected BSC-40 and VERO-E6 monolayers were fixed by adding 2 ml PBS/10% formaldehyde for 20 min at room temperature following by PBS rinse. The plates were then gamma-irradiated at the kill dose (4.4×10^6 rads) and removed from the BSL-4 laboratory for immunohistochemical staining. The monolayers were blocked in PBS/1% FBS overnight at room temperature and then incubated with 1 ml of rabbit anti-variola primary antibody (1:2000 dilution in PBS/1% FBS) for 30 min with gentle rocking. After two rinses with PBS followed by two 15 min washes with 1X PBS/Tween on an orbital rocker, 2 mls of goat anti-rabbit horseradish peroxidase conjugated secondary antibody diluted 1:2000 in PBS/1% FBS was added to each well and incubated for 30 min at room temperature with gentle rocking. After two rinses of PBS followed by one 15 min wash and a second 30 min wash with 1X PBS/Tween, plaques were visualized by adding 1 ml of the TrueBlue Peroxidase Substrate (KPL) to the monolayer for 10 minutes until developed. The developer was then removed and the monolayers were rinsed with water.

Figure S1 Dose response effect of CI-1033 on vaccinia IHDJ, WR and VGF deletion mutant (vSC20) plaque and comet formation. Immunohistochemical staining of BSC40 and VERO-E6 cells was performed as in Figure 3. *Effect of CI-1033 on vaccinia IHDJ plaque and comet*

formation 48 hours post infection. Note the 5-10 fold greater sensitivity of VERO-E6 to comet inhibition by CI-1033. Inset: Effect of CI-1033 on vaccinia WR and VGF deletion mutant (vSC20) plaque and comet formation 72 hours post infection in BSC40 cells. Note the overall smaller plaque phenotype and reduced comet formation of the VGF mutant.

Figure S2 The lungs from VV-infected mice were fixed in 10% neutral buffered formaldehyde and then paraffin-embedded. Tissue sections (5 μ m) were stained with hematoxylin and eosin. The scale bar represents 100 μ m. Control (infected but untreated) and various treatment groups are indicated. Note necrosis of bronchiolar cells and eosinophilic, acellular exudates in the control lung. By contrast, cellular infiltrates are evident in the CI-1033, the anti-L1R, and the CI-1033 + anti-L1R treatment groups. In the latter double treatment group, the bronchiolar epithelia are well preserved.

Figure S3 Host immune response to vaccinia pneumonia challenge during therapy. A) Cytokine expression profile of whole lungs from uninfected or infected (4,6 or 8) mice at indicated days post-infection analyzed by RNase protection assay. Day 8 virus-infected controls are lacking because the mice died. 6 μ g of total lung RNA from each mouse group was hybridized with the mCK-2b template set (BD Pharmingen) probes which are shown in the left-most lane and protected fragments visualized on a DNA sequencing gel. Note that shorter exposure of GAPDH and L32 hybridizing bands confirmed equivalence of sample loading (data not shown). B) IFN- γ producing CD8⁺ T cells in spleens of representative mice. Spleen cells from control, anti-L1R, CI-1033 or anti-L1R + CI-1033 treated infected mice (day 7) were stimulated in vitro by uninfected or VV-infected MC57G cells. Intracellular cytokine staining was performed and analyzed by flow cytometry. Numbers indicate the percentages of CD8 T cells. Methods for intracellular cytokine staining are as described (8).

Table S1. Lack of cytotoxicity of CI-1033 at various concentrations of BSC-40 monolayers.

	Experimental LDH Release (OD₄₉₀)	Maximum LDH Release (OD₄₉₀)	% Cytotoxicity
Untreated	-0.0485	2.8824	-1.6837
10 μM	0.0615	2.7341	2.2505
5 μM	0.0290	2.6394	1.0999
2.5 μM	0.0428	2.7960	1.5308
500 nM	0.0567	2.7315	2.0747
50 nM	-0.0048	2.6015	-0.1857

Cells were treated +/- CI-1033 at various concentrations for 48 hours and both supernatants and cell lysates were assayed for the presence of lactate dehydrogenase (LDH).

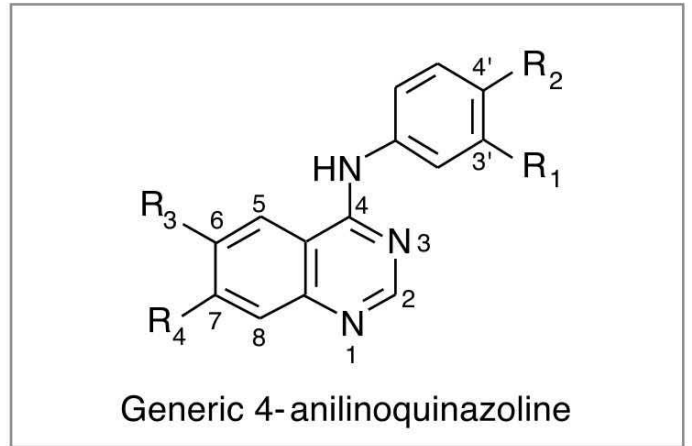
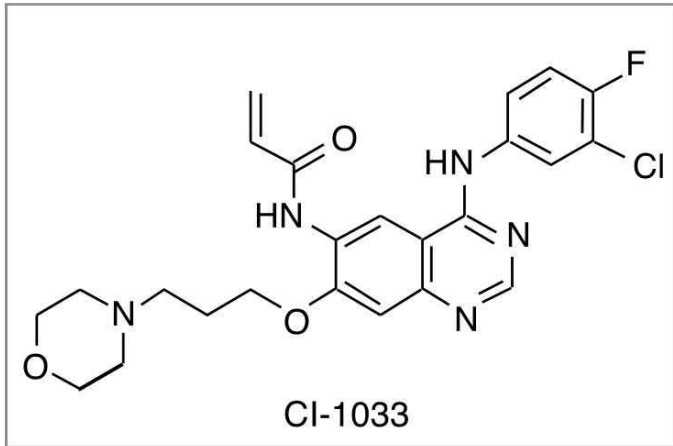
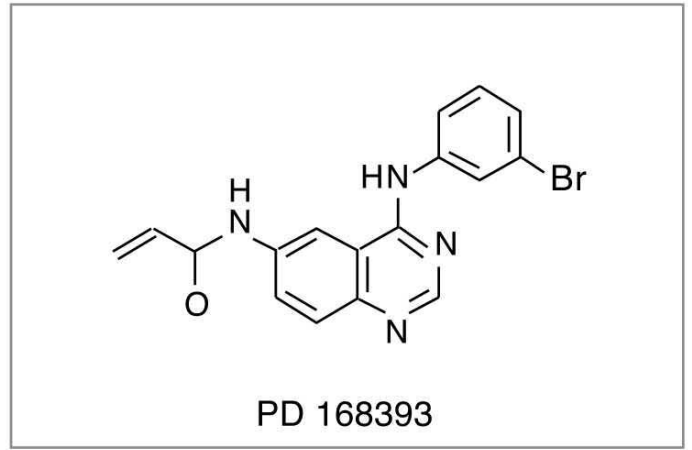
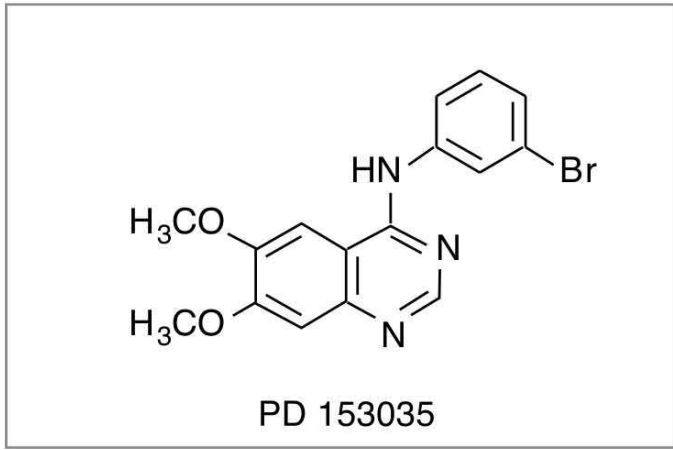
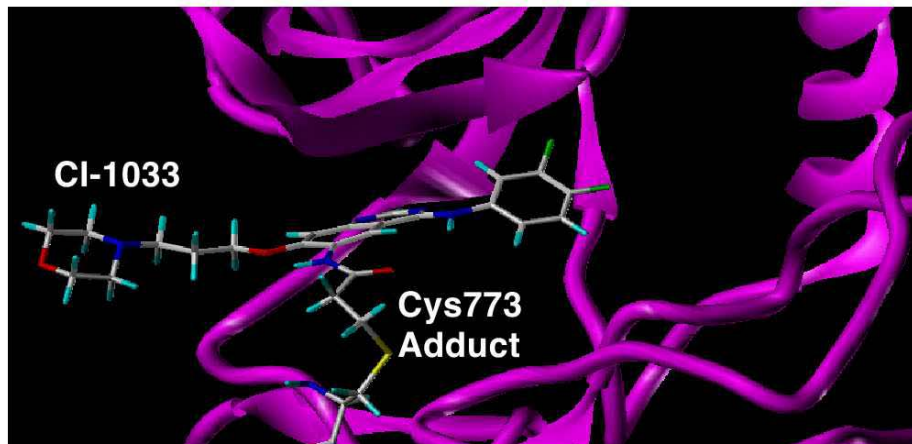
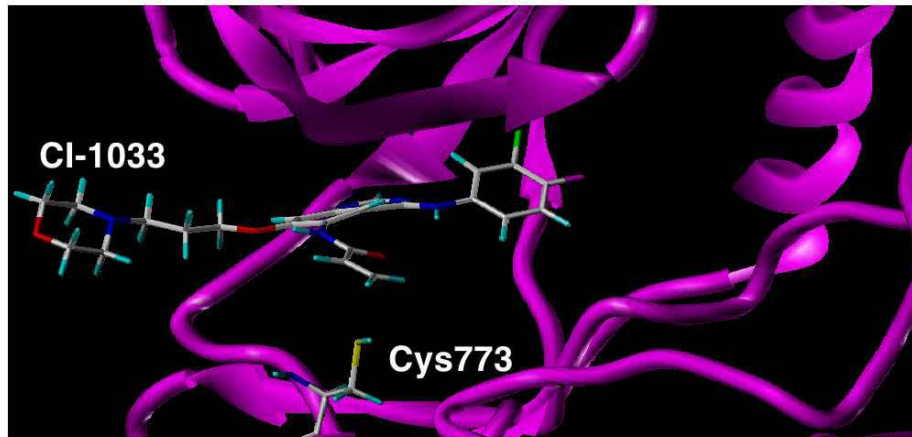
A**B**

Fig. 1

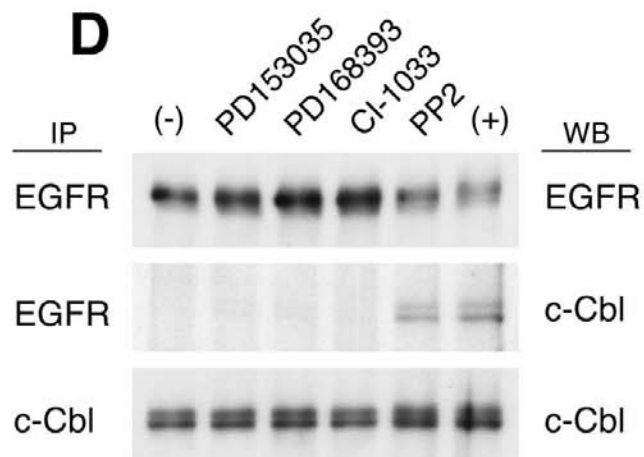
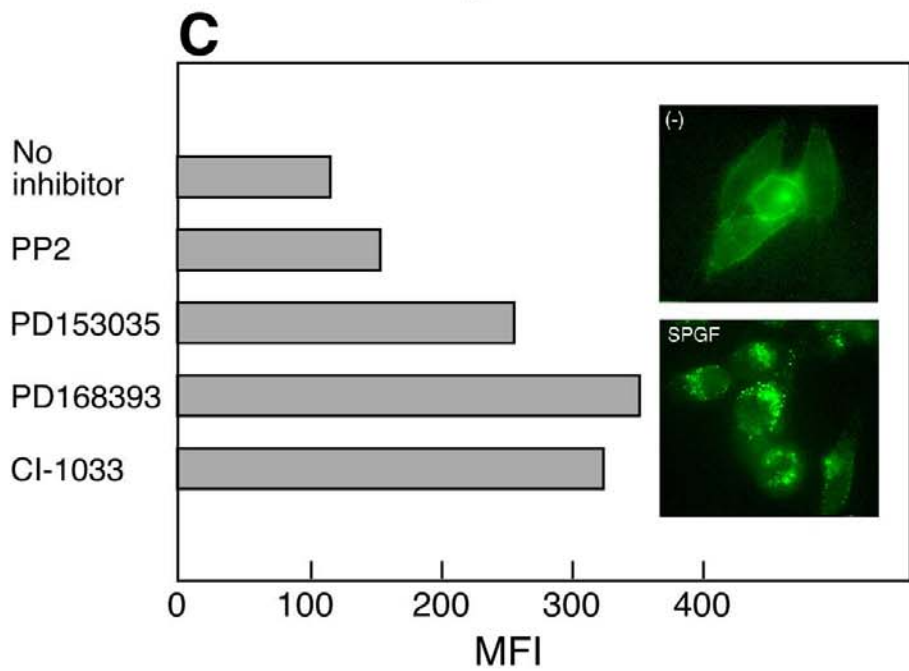
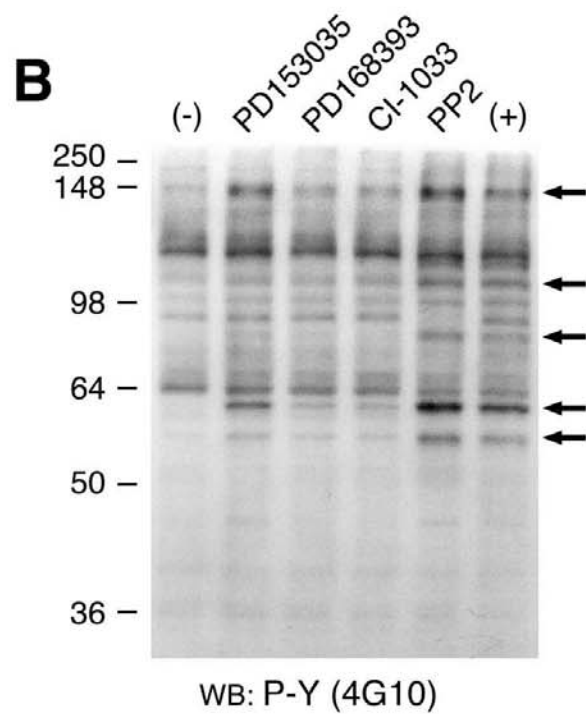
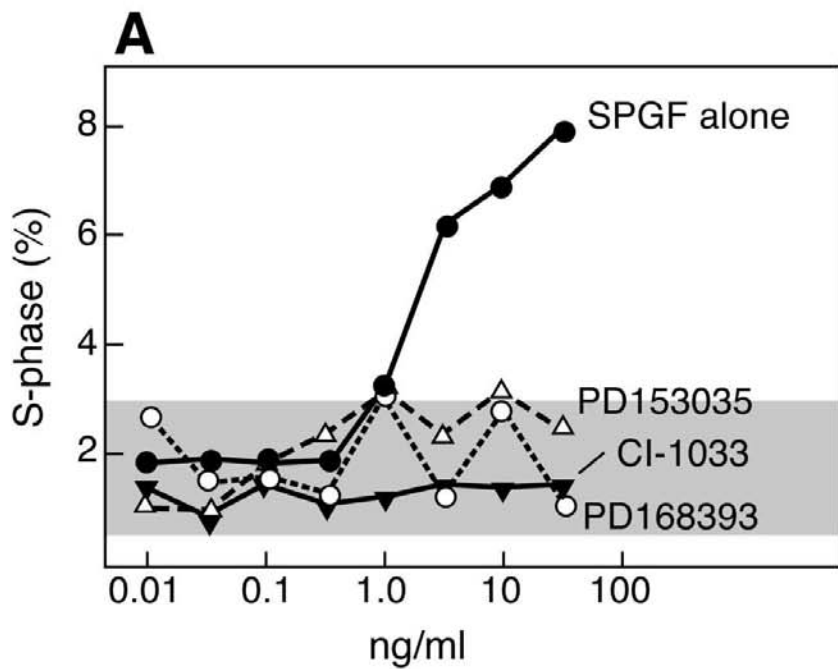


Fig. 2

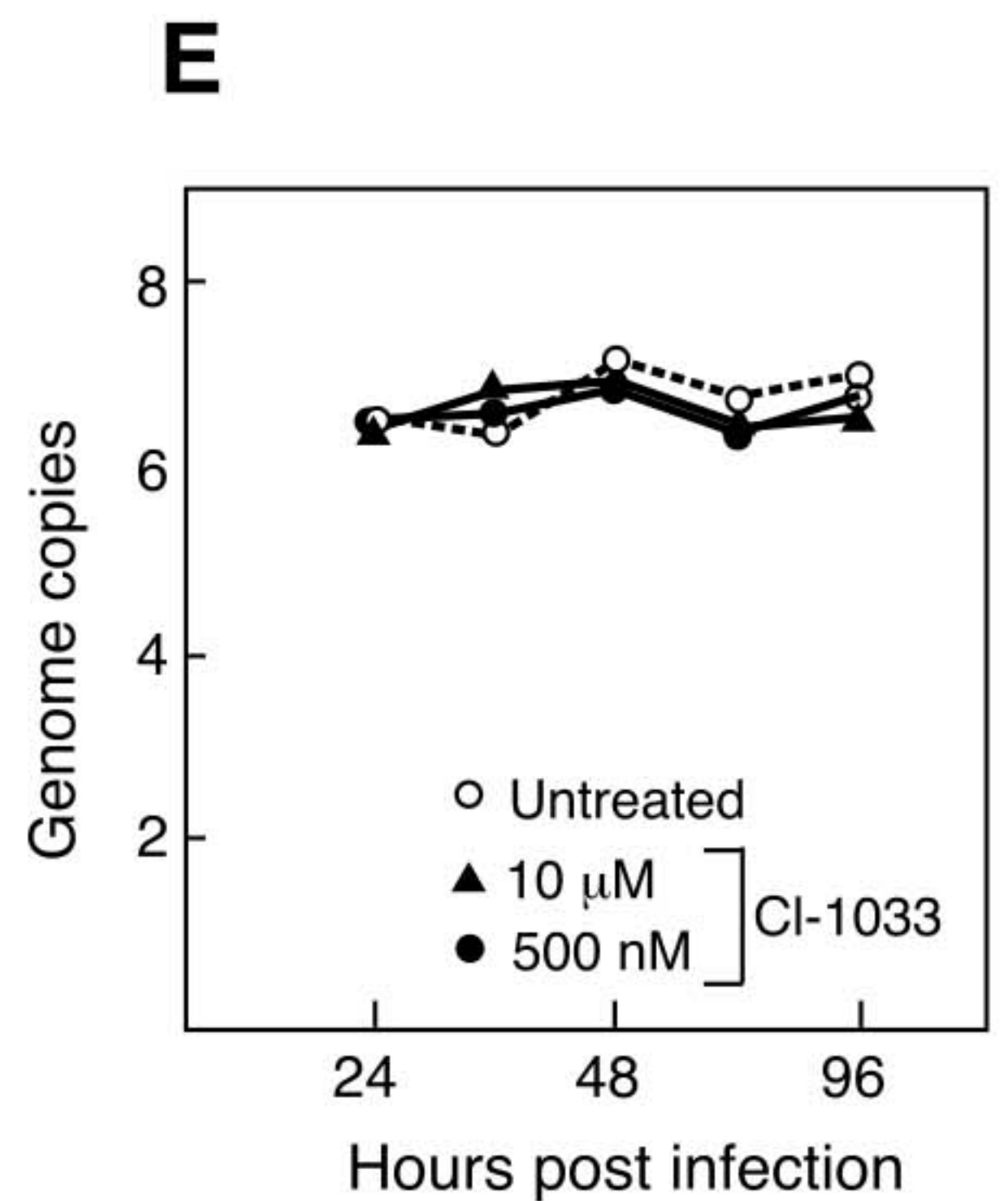
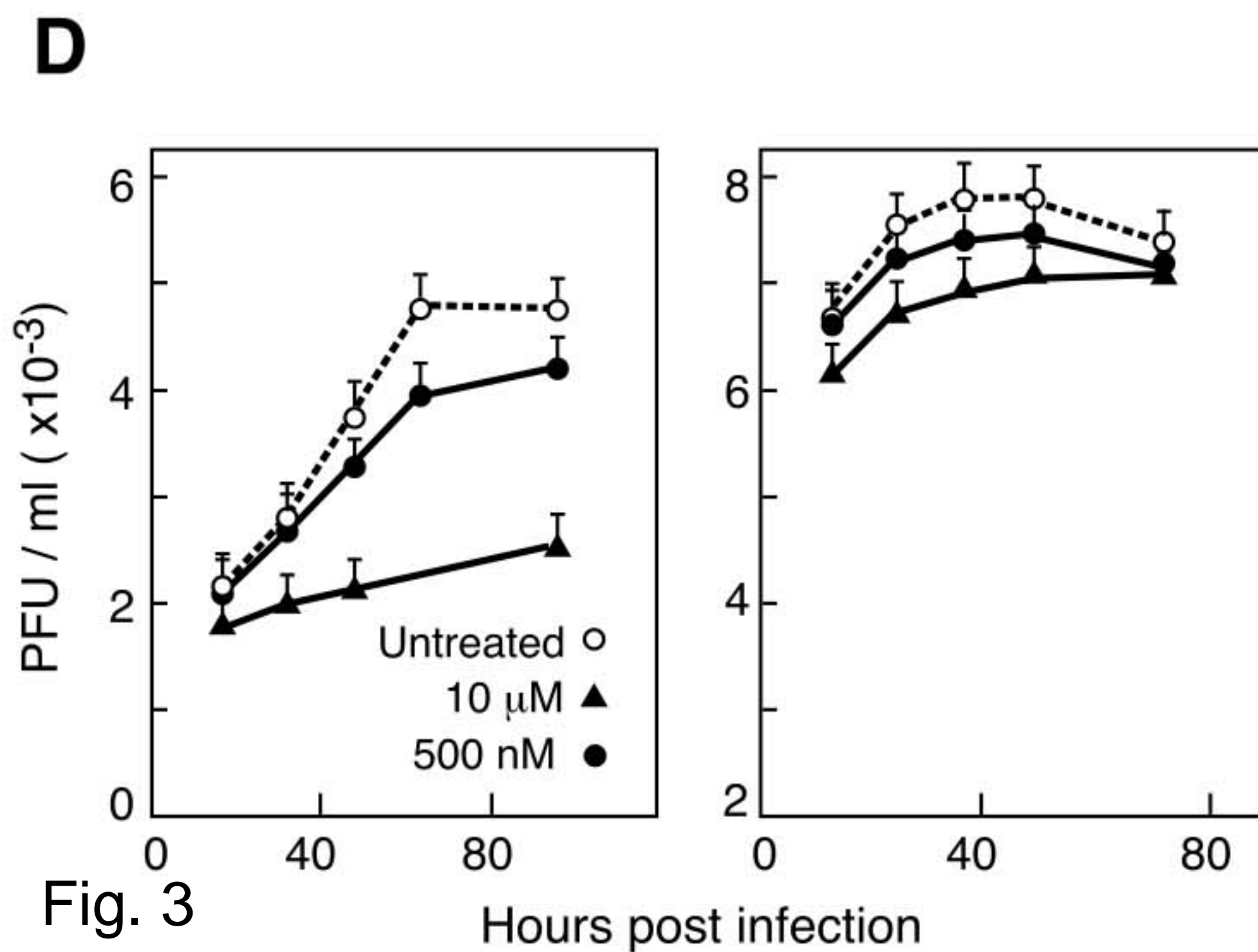
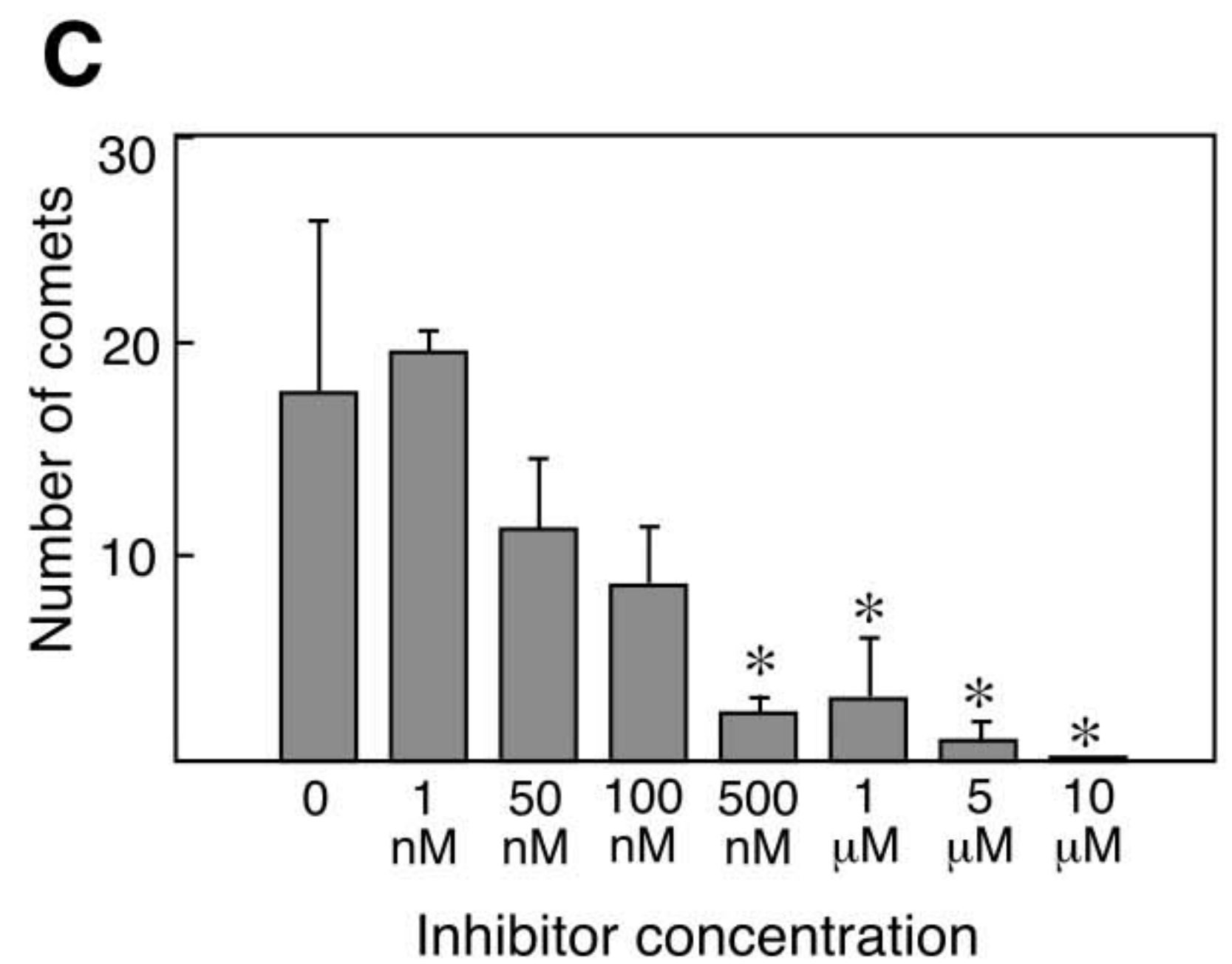
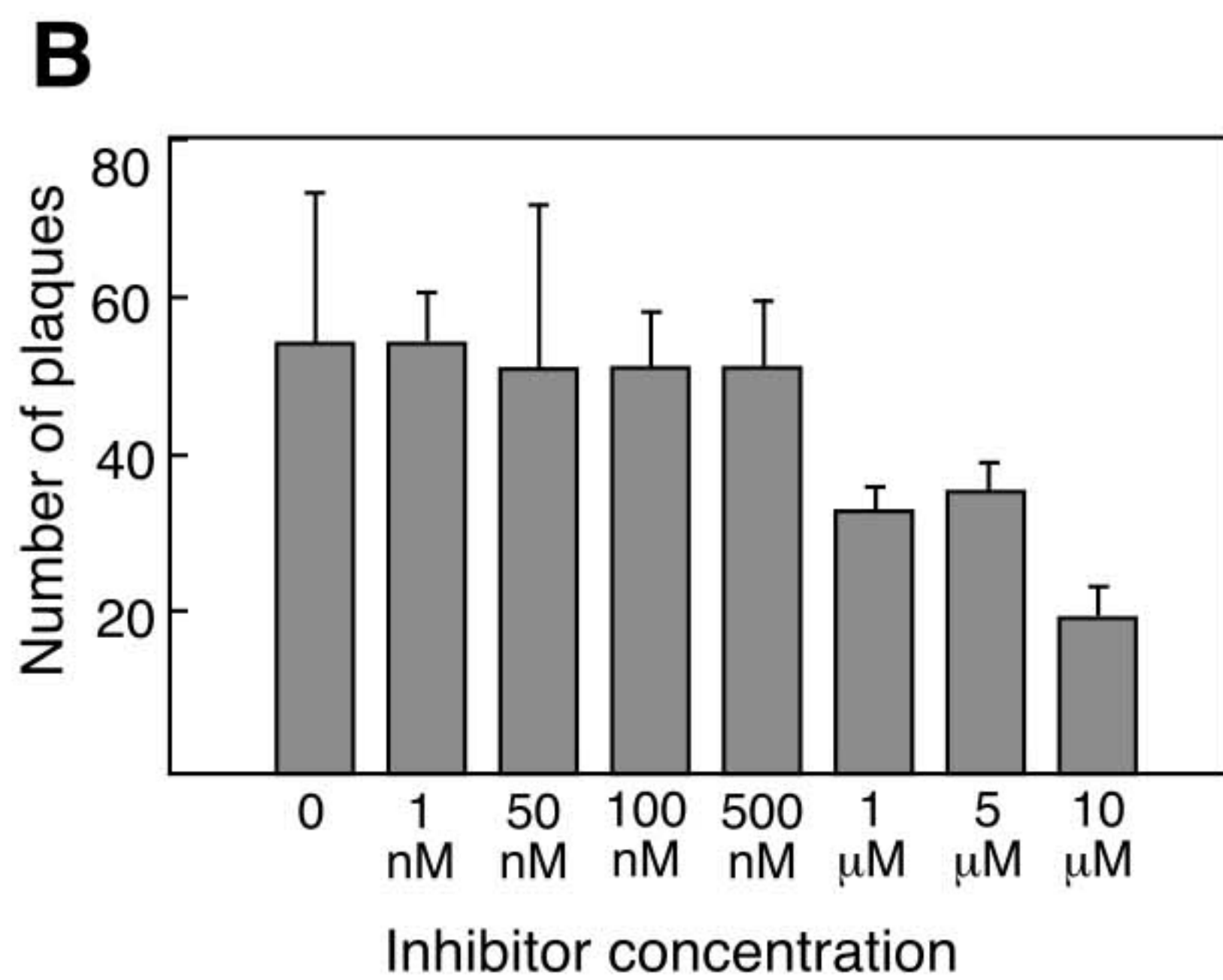
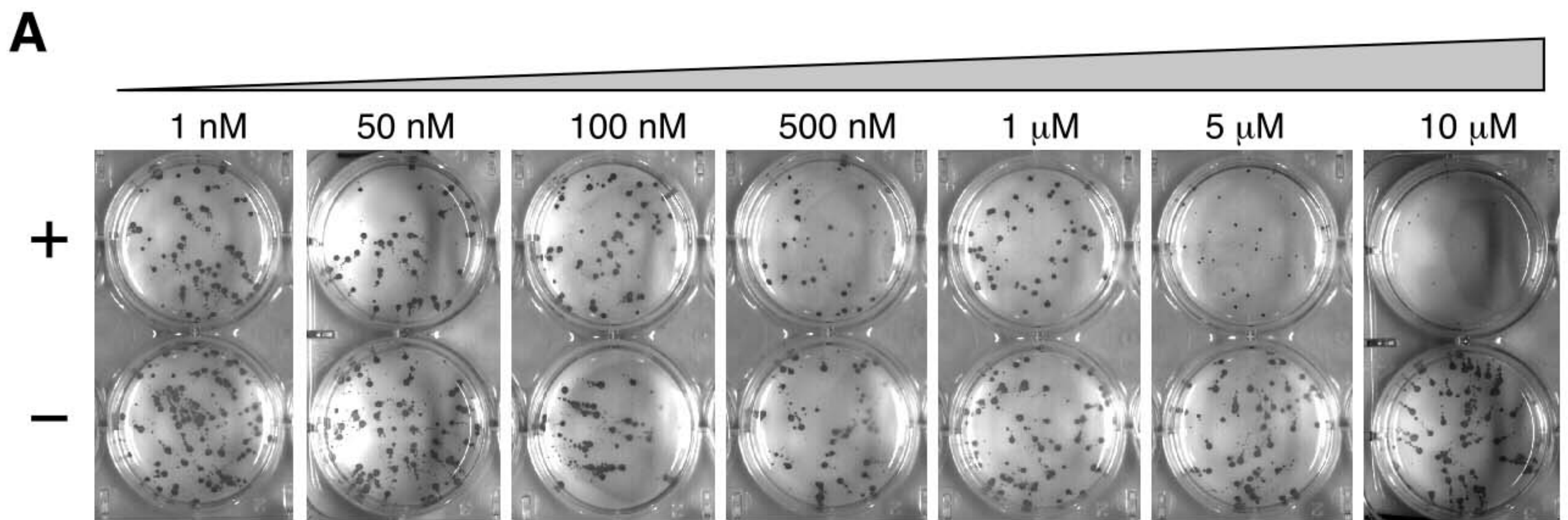


Fig. 3

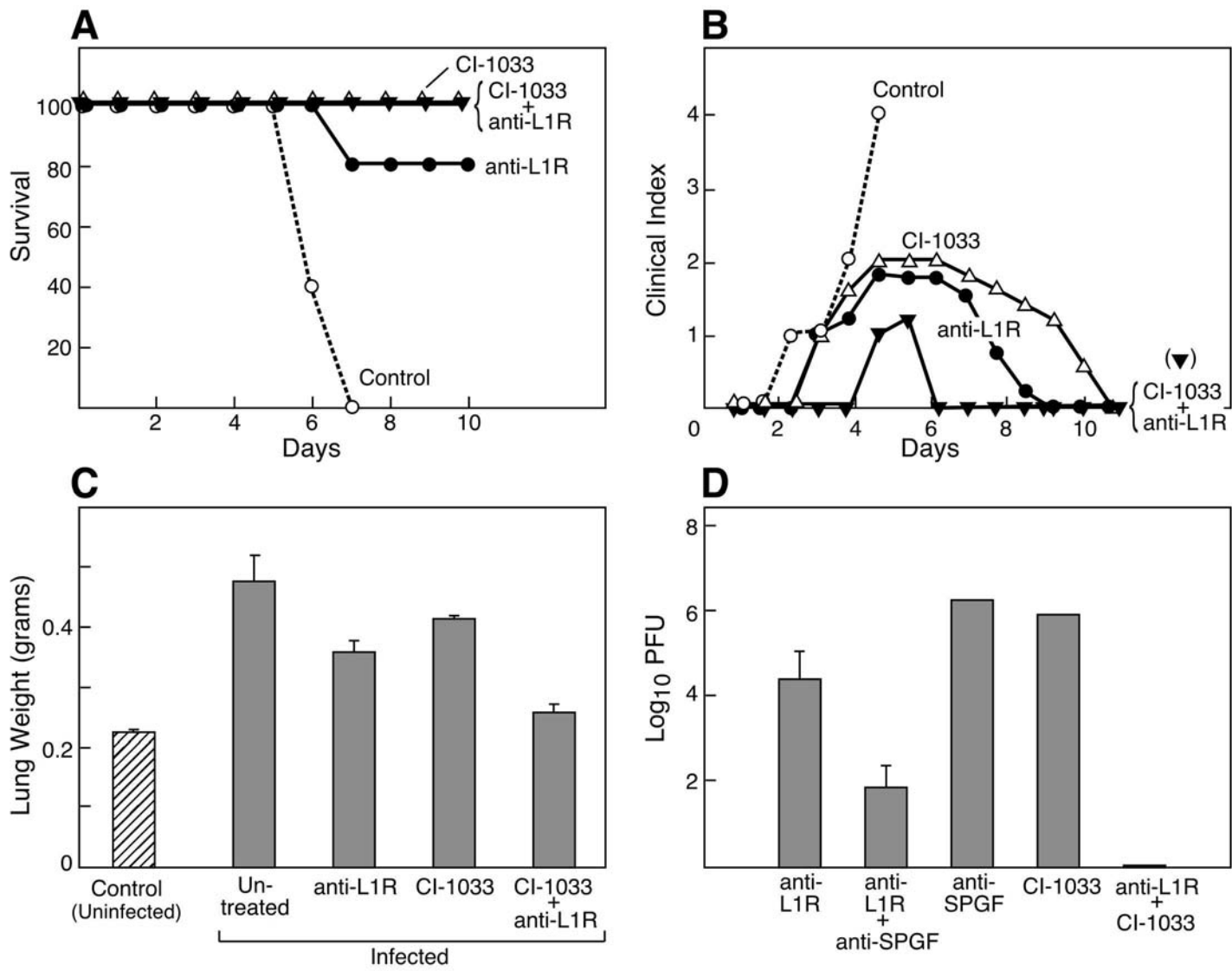


Fig. 4

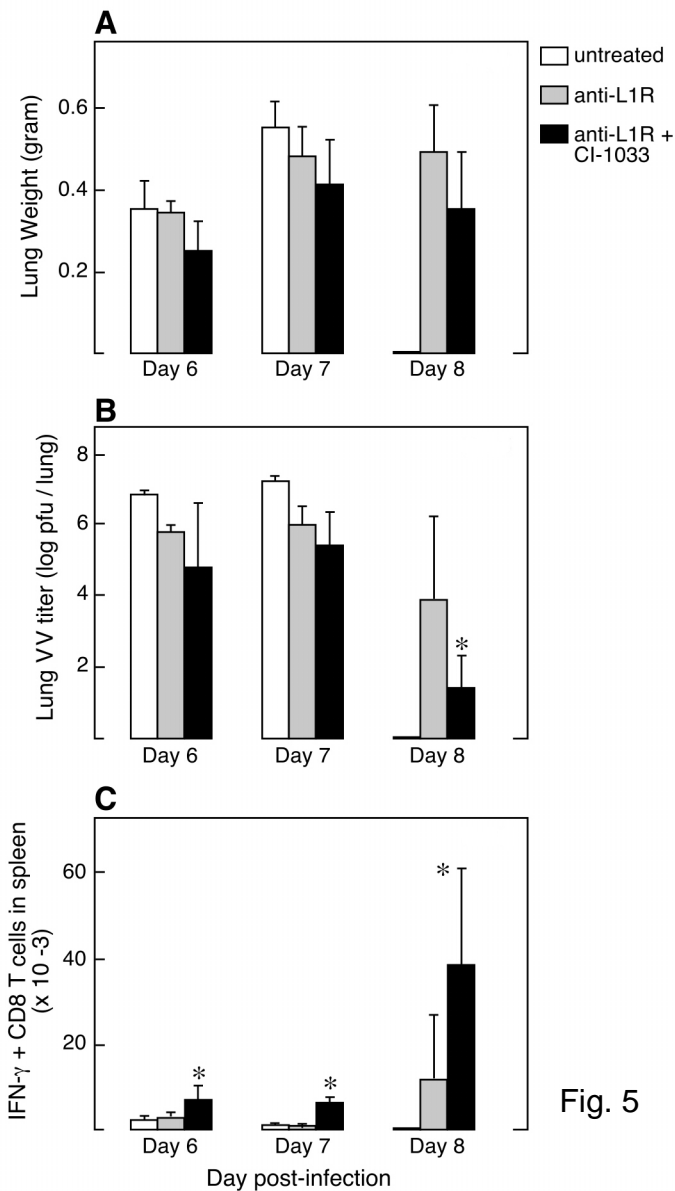


Fig. 5

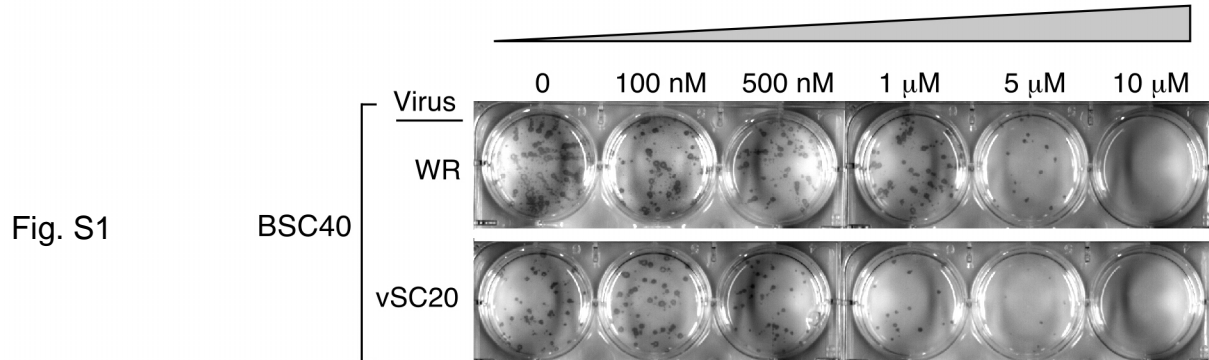
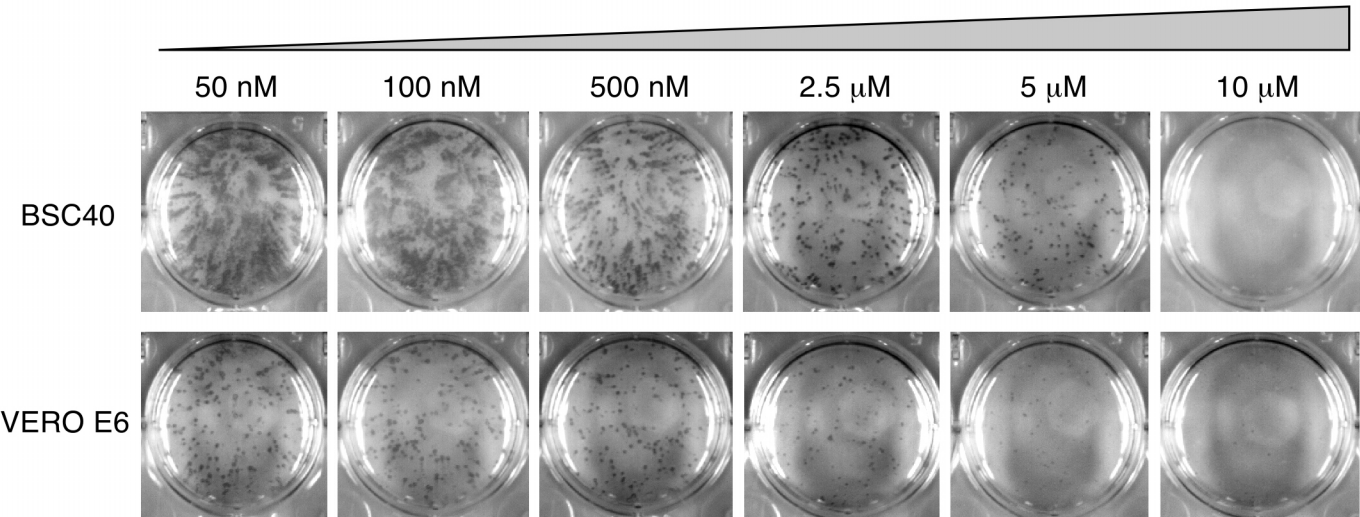
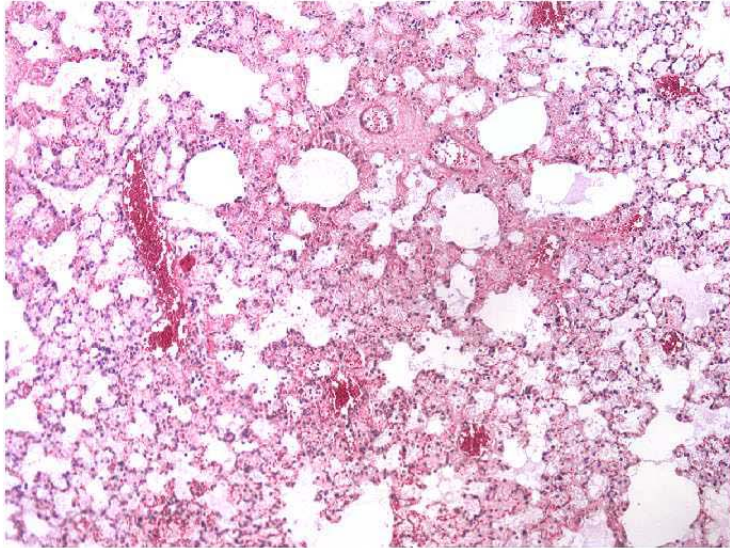
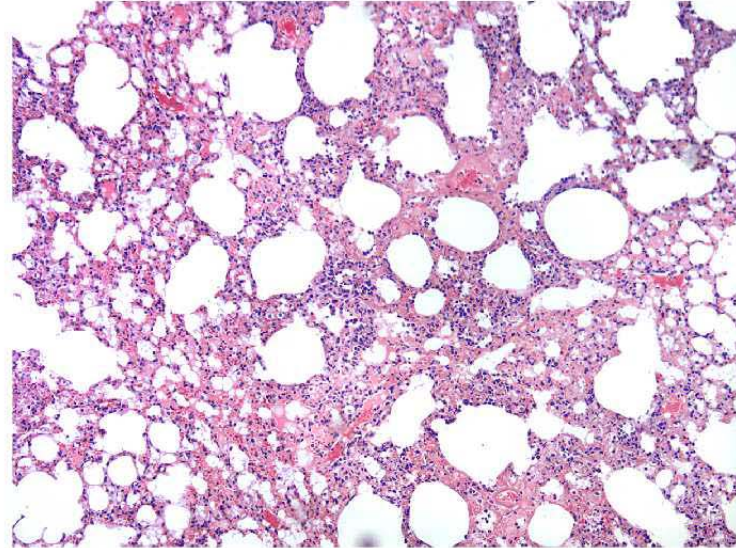


Fig. S1

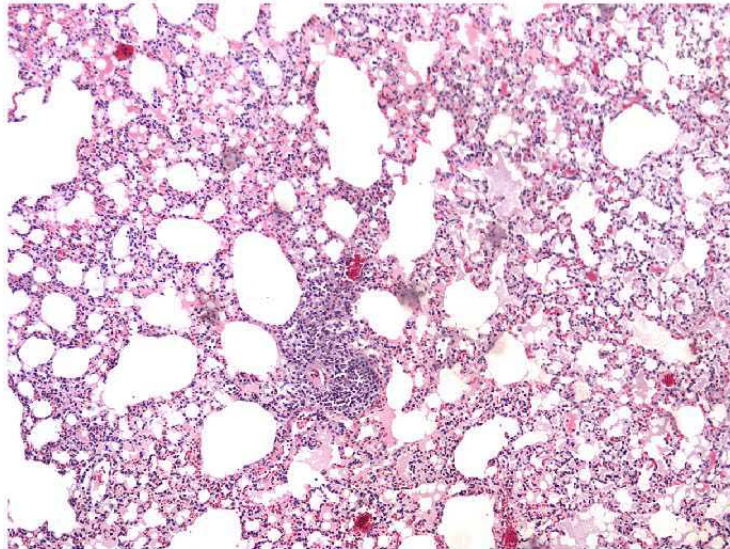
Control



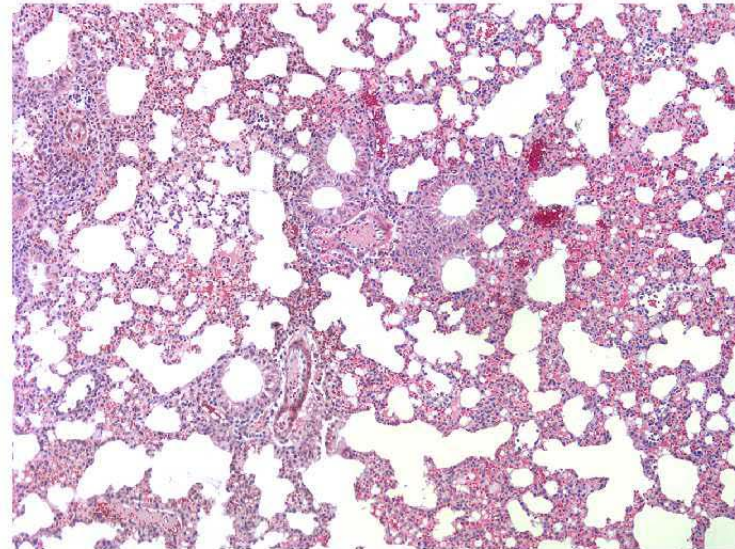
CI-1033



anti-L1R



CI-1033
+
anti-L1R



100 μ m

Fig. S2

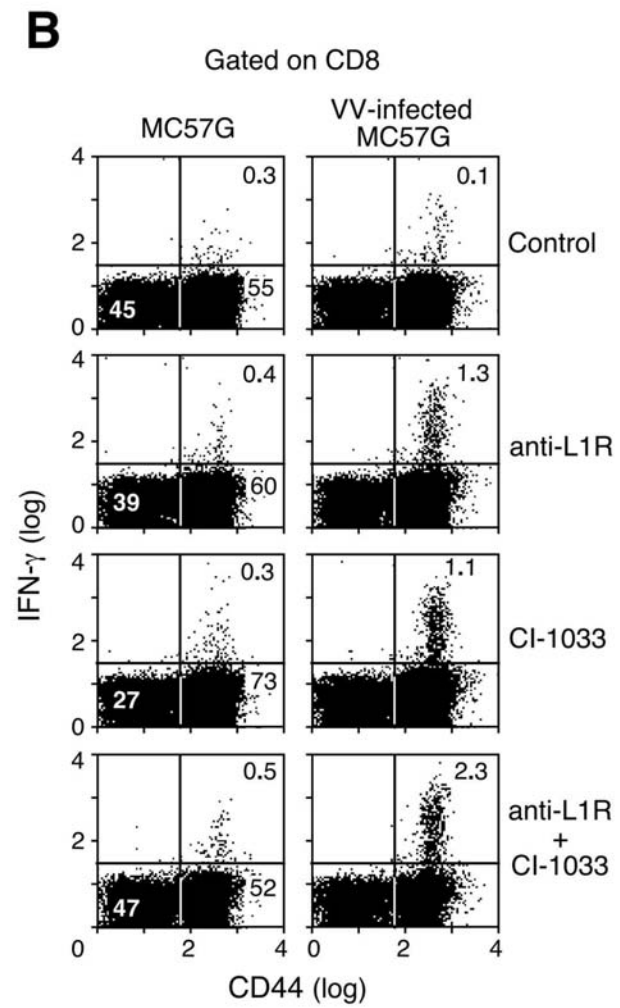
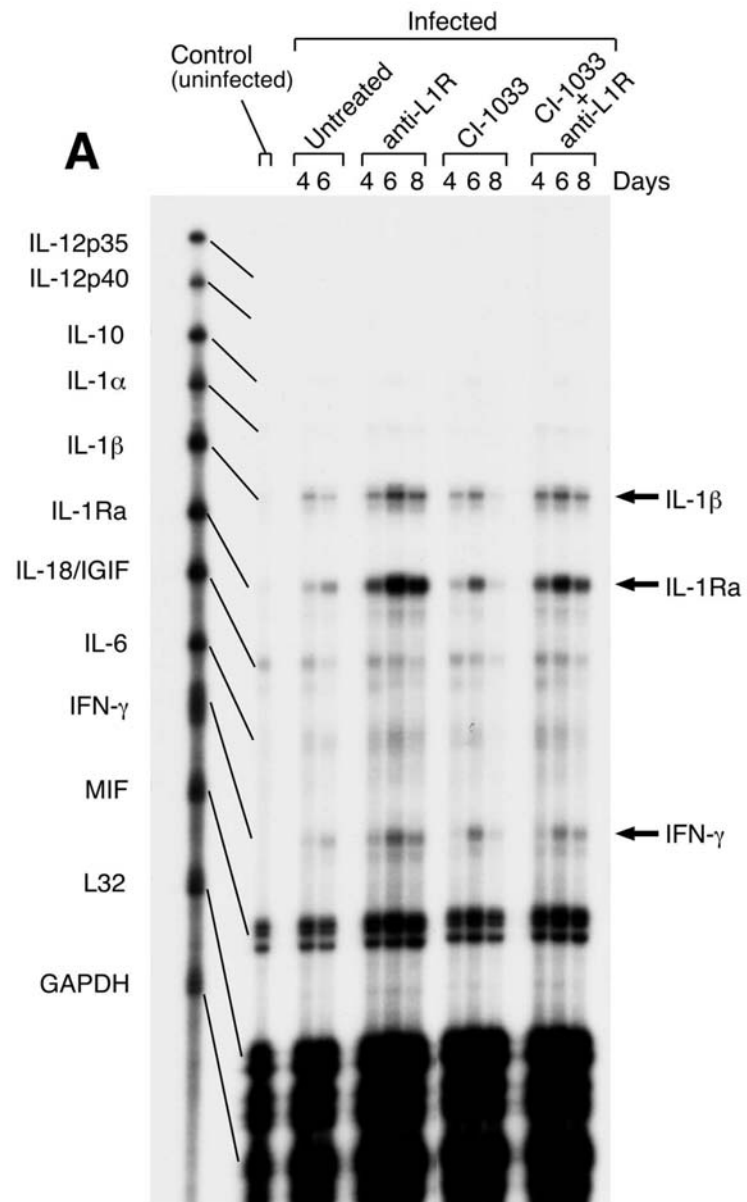


Fig. S3